

Review

Novel Radioligands for Cyclic Nucleotide Phosphodiesterase Imaging with Positron Emission Tomography: An Update on Developments Since 2012

Susann Schröder, Barbara Wenzel, Winnie Deuther-Conrad, Matthias Scheunemann and Peter Brust *

Department of Neuroradiopharmaceuticals, Institute of Radiopharmaceutical Cancer Research, Helmholtz-Zentrum Dresden-Rossendorf, Permoserstraße 15, Leipzig 04318, Germany; s.schroeder@hzdr.de (S.S.); b.wenzel@hzdr.de (B.W.); w.deuther-conrad@hzdr.de (W.D.-C.); m.scheunemann@hzdr.de (M.S.)

* Correspondence: p.brust@hzdr.de; Tel.: +49-341-234-179-4610

Academic Editor: Zhen Cheng

Received: 14 April 2016; Accepted: 10 May 2016; Published: 19 May 2016

Abstract: Cyclic nucleotide phosphodiesterases (PDEs) are a class of intracellular enzymes that inactivate the secondary messenger molecules, cyclic adenosine monophosphate (cAMP) and cyclic guanosine monophosphate (cGMP). Thus, PDEs regulate the signaling cascades mediated by these cyclic nucleotides and affect fundamental intracellular processes. Pharmacological inhibition of PDE activity is a promising strategy for treatment of several diseases. However, the role of the different PDEs in related pathologies is not completely clarified yet. PDE-specific radioligands enable non-invasive visualization and quantification of these enzymes by positron emission tomography (PET) *in vivo* and provide an important translational tool for elucidation of the relationship between altered expression of PDEs and pathophysiological effects as well as (pre-)clinical evaluation of novel PDE inhibitors developed as therapeutics. Herein we present an overview of novel PDE radioligands for PET published since 2012.

Keywords: positron emission tomography; phosphodiesterases; cyclic nucleotide signaling; PDE inhibitors; PDE radioligands; imaging

1. Introduction

Positron emission tomography (PET) is a powerful imaging technique in nuclear medicine for non-invasive *in vivo* localization of radiolabeled molecular probes (radiotracers). PET enables the quantitative kinetic measurement of physiological and biochemical processes by means of radiotracers labeled with short-lived positron emitting radionuclides, like fluorine-18 ($t_{1/2} = 109.8$ min), carbon-11 ($t_{1/2} = 20.4$ min), nitrogen-13 ($t_{1/2} = 9.98$ min), and oxygen-15 ($t_{1/2} = 2.03$ min). Hence, this method allows visualization of metabolic and transport processes, protein biosynthesis, and binding of ligands to specific receptors or enzymes [1]. PET imaging is widely used for diagnosis and (pre-)clinical research in oncology, neurology and cardiology [2–7].

The enzyme class of cyclic nucleotide phosphodiesterases (PDEs) consists of 11 families which differ in their amino acid sequences and thus in their three-dimensional structures, regulatory properties, distribution within the organism, intracellular expression and subcellular localization, as well as substrate specificity. PDEs degrade the secondary messenger molecules cyclic adenosine monophosphate (cAMP) and cyclic guanosine monophosphate (cGMP) due to hydrolysis of the phosphodiester bond of the cyclic phosphate group [8–10]. The dual-substrate specific PDE families 1, 2, 3, 10, and 11 inactivate both cAMP and cGMP while PDEs 4, 7, and 8 are cAMP selective and PDEs 5, 6, and 9 specifically hydrolyze cGMP. Signal transduction mediated by the cyclic nucleotides

affects various physiological processes like cell growth, differentiation and proliferation, metabolism, inflammation, and apoptosis [11–15]. The signaling cascades of cAMP and cGMP are affected by the PDEs altering the intracellular level of the respective cyclic nucleotide. Specific PDE inhibitors will raise the concentration of cAMP and/or cGMP and thus enhance cyclic nucleotide signaling. Hence, pharmacological inhibition of PDEs can provide a strategy for treatment of various diseases such as neurological, immune or inflammatory disorders, cancer, and heart diseases [9,14,16–22].

Therefore, appropriate PET radioligands for *in vivo* visualization and quantification of PDEs are of growing importance in clinical research to: (1) investigate the relationship between altered PDE expression and pathophysiological effects; and (2) provide a translational tool for evaluation of novel PDE inhibitors as therapeutics. The first PET radioligands described as imaging agents for a PDE enzyme were reported for the PDE4 family [23] and later found to be convenient for human application [24]. In the following ten years, development of further PET radioligands for the PDE families 1, 5, and 10 did not result in any suitable imaging agent for human use as extensively reviewed by Andrés *et al.* [25] in 2012. The herein presented overview is an update of the recently developed ¹¹C- and ¹⁸F-labeled radioligands for PET imaging of the PDEs 2, 4, 5, 7, and 10. So far no radioligands have been reported for the PDE family subtypes 3, 6, 8, 9, and 11.

2. PDE2 Radioligands

Phosphodiesterase 2 (PDE2) is a member of the dual-substrate specific PDE family degrading both cAMP and cGMP [26]. The enzyme is encoded by the gene *PDE2A* and expressed in three isoforms. These isoforms differ in their N-terminal amino acid sequence and in their intracellular localization: PDE2A1 is a cytosolic protein, whereas PDE2A2 as well as PDE2A3 are membrane-associated [20,27,28]. Regarding enzyme kinetics, there are no differences known between the three isoforms [14]. PDE2A activity is regulated by allosteric binding of cGMP at the regulatory subunits that induces a conformational change of the catalytic domain resulting in accessible substrate binding sites in the active center [29–32].

The PDE2A protein is mainly expressed in the brain and only at low levels in certain peripheral tissues such as spleen, adrenal gland, heart, liver, kidney, lung, and small intestine [9,33–36]. In addition, this enzyme is expressed in particular tumors, for instance malignant melanoma cells [37,38], adrenocarcinoma [39], and mammary carcinoma [40]. In the brain, PDE2A is highly expressed in cortex, hippocampus, striatum, substantia nigra, globus pallidus, habenulae, bulbus olfactorius, tuberculum olfactorium, and amygdala [41,42]. The specific localization in structures of the limbic system indicates a modulation of important neuronal functions associated with emotion, learning, and memory [41,43–47]. Therefore, it is assumed that PDE2A is involved in the pathophysiology of neuropsychiatric and neurodegenerative disorders, such as depression and Alzheimer's disease [42,48,49].

Pharmacological inhibition of PDE2A leads to an increase of the intracellular levels of cAMP and cGMP and is suggested to improve neuronal plasticity [43,49–53]. Thus, PDE2A inhibitors are considered as a promising approach for treatment of related neurological diseases [43,48–51,54]. Accordingly, development of specific PET radioligands for *in vivo* imaging and quantification of PDE2A has been recently gaining in importance in brain research (www.clinicaltrials.gov: NCT02584569).

In 2013, the first two ¹⁸F-labeled PDE2A radioligands have been published by Janssen Pharmaceutica NV, [¹⁸F]1 ([¹⁸F]B-23) [48,55], and Pfizer Inc., [¹⁸F]2 ([¹⁸F]PF-05270430) [48,56] (Figure 1). The triazoloquinoxaline derivative 1 [48,55] is of high inhibitory potency towards the PDE2A protein, but of low PDE2A/PDE10A selectivity ($IC_{50}(PDE2A) = 1 \text{ nM}$; $IC_{50}(PDE10A) = 11 \text{ nM}$). Notably, the distribution pattern of PDE2A and PDE10A is comparable: both enzymes are highly expressed in the caudate nucleus as a part of the striatum [34]. For that reason, high selectivity of PET radioligands towards PDE2A is substantially for specific imaging of this enzyme. The ¹⁸F-labeled analogue [¹⁸F]1 has been synthesized in a one-step nucleophilic aromatic radiolabeling strategy by using the related nitro precursor and $K^+ / [^{18}F]F^- / K_{2.2.2}$ -carbonate complex under microwave heating [55]

(Scheme 1). In biodistribution and microPET imaging studies with rats, the highest accumulation of [^{18}F]1 at 2 min post injection has been observed in striatum followed by hippocampus, cortex, and cerebellum [55]. However, the reported specific uptake in the striatum may be caused by binding of [^{18}F]1 to PDE2A and PDE10A in this brain region as a result of its low selectivity. Additionally, polar radiometabolites have been detected in the brain with 4% of total activity at 2 min up to 18% at 10 min post injection [55]. In conclusion, [^{18}F]1 appears not to be an appropriate radioligand for *in vivo* imaging of the PDE2A protein.

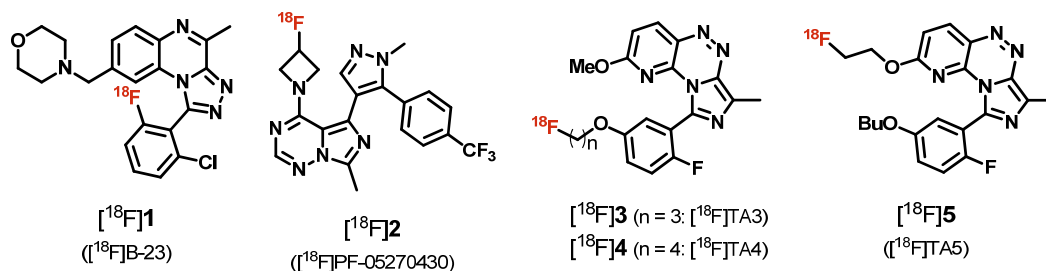
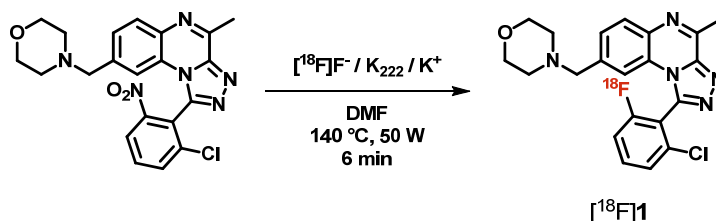


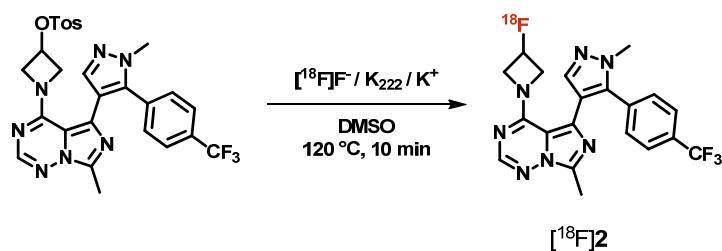
Figure 1. Molecular structures of ^{18}F -labeled PDE2A inhibitors for PET.



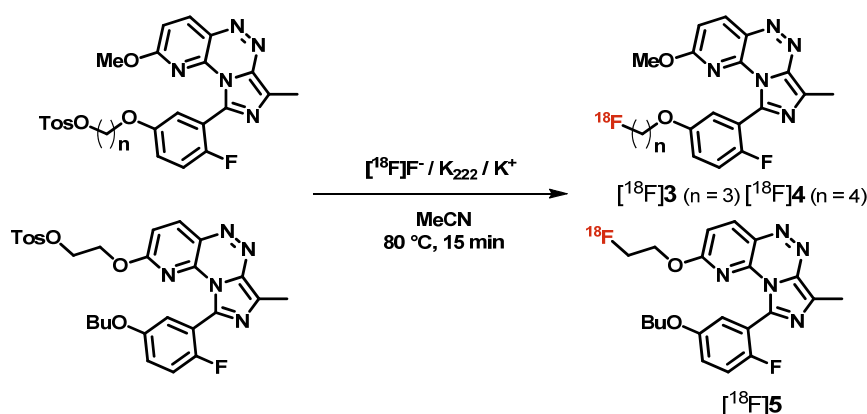
Scheme 1. Radiosynthesis of [^{18}F]1.

The PDE2A inhibitor 2 (PF-05270430) [48,56] has been developed out of a series of imidazolotriazine compounds and is of high potency and selectivity towards PDE2A ($\text{IC}_{50}(\text{PDE2A}) = 0.5\text{ nM}$; $\text{IC}_{50}(\text{PDE10A}) > 3000\text{ nM}$) with good brain uptake. The radioligand [^{18}F]2 has been prepared initially by nucleophilic aliphatic displacement of the tosylate group of the corresponding precursor with tetra-*n*-butylammonium [^{18}F]fluoride in *tert*-amyl alcohol [56]. In order to increase the radiochemical yield of [^{18}F]2 from $< 2\%$ [56] up to 20%, an optimized radiosynthesis procedure by using $\text{K}^+ / [^{18}\text{F}]\text{F}^- / \text{K}_{2.2.2}$ -carbonate complex in dimethyl sulfoxide under GMP-compliant conditions has been developed by Morley *et al.* [57] (Scheme 2). In PET studies on monkeys a rapid and high uptake of [^{18}F]2 in striatum and low uptake in cerebellum has been reported, consistent with the distribution pattern of the PDE2A in brain [35,41]. Furthermore, no defluorination has been observed and an effective blocking of radioligand accumulation in the striatum has been described [56]. Notably, [^{18}F]2 has already been evaluated in first human PET studies in healthy volunteers as reported in a conference abstract in 2013 [58] and very recently in a detailed publication by Naganawa *et al.* [59]. The results of these studies indicate that [^{18}F]2 is suitable for PET imaging of PDE2A in the human brain based on the observed radioligand accumulation in PDE2A-specific brain regions, the favorable kinetic profile, the high tolerability and safety as well as the good metabolic stability [59].

Besides [^{18}F]1 and [^{18}F]2, three ^{18}F -labeled imidazopyridotriazine derivatives as potential PDE2A radioligands for PET, [^{18}F]3, [^{18}F]4, and [^{18}F]5 ([^{18}F]TA3–5, Figure 1), have been developed in our group [60–62] based on a patented lead compound [43].

Scheme 2. Radiosynthesis of $[^{18}\text{F}]\text{2}$.

The non-radioactive fluoroalkoxyphenyl derivatives **3** and **4** are of high inhibitory potency and selectivity towards PDE2A (**3**: $\text{IC}_{50}(\text{PDE2A}) = 11 \text{ nM}$; $\text{IC}_{50}(\text{PDE10A}) = 318 \text{ nM}$; **4**: $\text{IC}_{50}(\text{PDE2A}) = 7 \text{ nM}$; $\text{IC}_{50}(\text{PDE10A}) = 913 \text{ nM}$) [61]. In addition, replacement of the methoxy group at the pyridinyl moiety of the lead compound by a fluoroethoxy side chain resulted in the most potent derivative out of this series, compound **5**, with a significantly increased PDE2A/PDE10A selectivity ($\text{IC}_{50}(\text{PDE2A}) = 3 \text{ nM}$; $\text{IC}_{50}(\text{PDE10A}) > 1000 \text{ nM}$) [62]. The radioligands $[^{18}\text{F}]\text{3}$, $[^{18}\text{F}]\text{4}$, and $[^{18}\text{F}]\text{5}$ have been prepared in a one-step radiosynthesis by nucleophilic aliphatic substitution of the tosylate group of appropriate precursors with the anhydrous $\text{K}^+ / [^{18}\text{F}]\text{F}^- / \text{K}_{2,2,2}$ -carbonate complex [61,62] (Scheme 3). *In vitro* autoradiography on rat brain slices displayed region-specific binding of $[^{18}\text{F}]\text{3}$ and $[^{18}\text{F}]\text{4}$ [61,62], which is consistent with the PDE2A distribution pattern in rat brain [34,41] and could be blocked by co-incubation with the lead compound. In autoradiographic studies with $[^{18}\text{F}]\text{5}$ on sections of rat and pig brain, a homogenous and non-displaceable distribution of activity has been detected indicating high non-specific binding of this radioligand (unpublished work). Small-animal PET studies with $[^{18}\text{F}]\text{3}$ in mice showed a fast wash out of activity from the striatum while a constantly increased uptake in the non-target region cerebellum has been observed [61,62]. This finding likely reflects the accumulation of brain penetrating radiometabolites which has been confirmed in metabolism studies with $[^{18}\text{F}]\text{3}$, $[^{18}\text{F}]\text{4}$, and $[^{18}\text{F}]\text{5}$ where 29%, 4% [61], and 10%, respectively, of total activity in the mouse brain have been represented by the intact radioligands at 30 min post injection. It is suggested that cytochrome P450 enzyme induced metabolic degradation of the ^{18}F -bearing alkyl side chains in $[^{18}\text{F}]\text{3}$ –**5** resulted in formation of the corresponding brain penetrating ^{18}F -alkyl alcohols, aldehydes or carboxylic acids [61,63,64].

Scheme 3. Radiosyntheses of $[^{18}\text{F}]\text{3}$, $[^{18}\text{F}]\text{4}$, and $[^{18}\text{F}]\text{5}$.

Overall, we have concluded that none of the up to now generated ^{18}F -labeled imidazopyridotriazine derivatives meets the requirements for PET imaging of PDE2A in the brain. Nevertheless, further structural modification of these promising radioligands is currently in progress and might result in metabolically stable derivatives.

3. PDE4 Radioligands

Up to now, phosphodiesterase 4 (PDE4) is one of the most studied PDE families. This enzyme specifically hydrolyses cAMP and is expressed by four genes *PDE4A*, *B*, *C*, and *D* that generate overall more than 20 isoforms [65,66]. The different genes vary in their coding sequences for the C- and N-terminus of the enzyme and the numerous isoforms are characterized by distinct regulatory subunits [9,20,35,67]. In general, PDE4 is expressed in a wide range of tissues and cell types, such as brain, smooth muscle, heart, lung, kidney, endothelium and immune cells [9,20,34,67]. In the periphery, PDE4B and PDE4D are the most abundant PDE4 mRNAs with highest levels of PDE4B in spleen, lung, and bladder and of PDE4D also in bladder as well as skeletal muscle, and thyroid [34]. Regarding mRNA levels in brain, PDE4B is the most abundantly expressed PDE4, with highest levels in hypothalamus, followed by PDE4A and PDE4D. By comparison, PDE4C shows the lowest expression in both peripheral and brain tissues [34,68].

PDE4 activity is suggested to be involved in several processes such as brain function primarily associated with mood changes [69], monocyte [70] and macrophage activation [71], neutrophil infiltration [72], and vascular smooth muscle proliferation [73]. Thus, PDE4 inhibitors are of great interest for treatment of neurological disorders, including depression, Alzheimer's disease, and disorders of the immune and inflammatory system, particularly chronic obstructive pulmonary disease and asthma [9,20,32,67,68,74]. The main drawback of the early developed PDE4 inhibitors has been emesis as one side effect of these compounds because of low selectivity towards the different PDE4 isoforms [9,32,67]. To overcome this problem, second generation compounds, like cilomilast, have been identified with reduced side effects liability [75].

The most extensively studied PDE4 inhibitor **6** (rolipram, Figure 2) leads to an increase in cerebral cAMP levels and is known as potent antidepressant but side effects have hampered clinical application [20,67]. It has been reported that rolipram inhibits the PDE4A, B, C and D isoforms at a similar degree [76], while other studies showed differences [77,78]. However, the ^{11}C -labeled analogue of (*R*)-**6** (^{11}C]rolipram) [79] has been suggested as a promising PET radioligand for *in vivo* evaluation of PDE4 levels and alterations in cAMP signaling pathways [24] as already reviewed elsewhere [25,67]. Meanwhile, ^{11}C]6 has successfully been used to demonstrate downregulation of PDE4 in major depressive disorder [80] and to monitor progression of certain cardiac disorders such as heart failure, mitral valve disease, diabetic cardiomyopathy, and adriamycin cardiotoxicity [81].

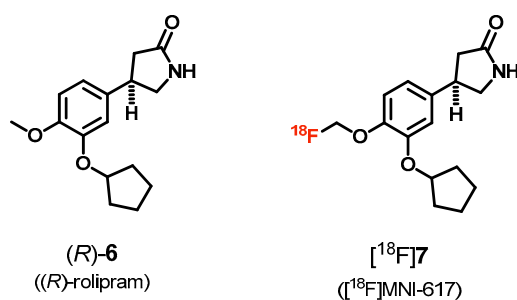
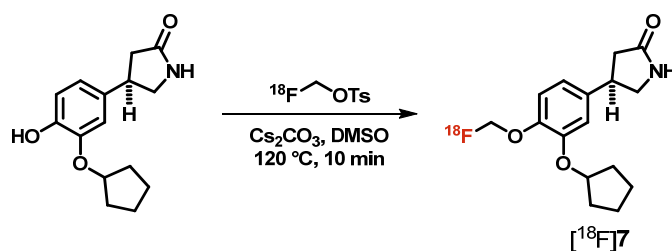


Figure 2. Molecular structures of PDE4 inhibitor (*R*)-**6** and the ^{18}F -analogue thereof for PET.

Very recently, Thomae *et al.* [82,83] reported on the development of structurally modified derivatives of (*R*)-**6** with the aim to generate ^{18}F - and ^{123}I -labeled PDE4 radioligands for PET or SPECT application, respectively. In general, low tolerance of PDE4 for structural changes in (*R*)-**6** has been stated as well as a significant decrease in PDE4 affinity for the iodo derivatives that consequently have been suggested to be not suitable as SPECT radioligands. Out of this series, the fluorinated analogue **7** (MNI-617, Figure 2) has been described as the most promising compound with a five-fold increased PDE4 affinity over (*R*)-**6** ($K_D = 0.26$ nM *vs.* 1.6 nM) and thus has been selected for ^{18}F -labeling [82,83].

Initially, [^{18}F]7 has been prepared in an one-pot two-step radiosynthesis procedure via ^{18}F -labeling of diiodomethane using $\text{K}^+ / [^{18}\text{F}]\text{F}^- / \text{K}_{2,2,2}$ -carbonate complex followed by *O*-alkylation of the corresponding phenol precursor with the resulting [^{18}F]fluoroiodomethane [82]. At the 21st International Symposium on Radiopharmaceutical Sciences, Columbia 2015, the group has presented an optimized two-step radiolabeling strategy by first generating [^{18}F]fluoromethane tosylate that has been used as a prosthetic group for subsequent *O*-alkylation of the phenol precursor under basic conditions (Scheme 4). In this radiosynthesis, the overall radiochemical yield of [^{18}F]7 has been increased from 1.5% up to 29%. In PET studies on monkeys a fast and high uptake of [^{18}F]7 in the brain has been observed, with specific distribution in regions of known PDE4 expression [82,83]. Although no data concerning the metabolic stability of [^{18}F]7 have been published yet, the authors stated that the [^{18}F]fluoromethyl group might be defluorinated *in vivo* leading to bone uptake of the resulting free [^{18}F]fluoride [83] which is indeed a known process in the metabolism of ^{18}F -alkylated radioligands. Thus, the group also synthesized and evaluated the deuterated analogue D_2 -[^{18}F]7 (D_2 -[^{18}F]MNI-617) [83,84]. PET studies in monkeys with D_2 -[^{18}F]7 revealed a comparable brain distribution and kinetic profile like [^{18}F]7. However, accumulation of activity in the skull indicates fast defluorination of D_2 -[^{18}F]7 [83]. Despite the high and PDE4-specific brain uptake as well as the favorable brain kinetics of [^{18}F]7 and D_2 -[^{18}F]7, it has been concluded that these radioligands are not suitable for PET imaging of PDE4 because of their low metabolic stability [83].



Scheme 4. Radiosynthesis of [^{18}F]7.

4. PDE5 Radioligands

The cGMP specific phosphodiesterase 5 (PDE5) is a cytosolic protein activated by allosteric binding of cGMP [85,86]. This enzyme is encoded by the gene *PDE5A* and is expressed as three isoforms, PDE5A1, PDE5A2, and PDE5A3 that differ in their N-termini. It is assumed that PDE5A expression is regulated by the specific promoter sequences of these isoforms [87]. PDE5A1 and PDE5A2 are widely distributed in numerous tissues such as bladder, lung, stomach, thyroid, pancreas, heart, intestine, vascular smooth muscle and at low levels in brain, whereas PDE5A3 is specifically expressed in vascular smooth muscle [9,34,87]. It is well known that PDE5A regulates vascular smooth muscle contraction by controlling the intracellular cGMP level, especially in penis and lung. Thus, pharmacological inhibition of PDE5A activity is in clinical application for treatment of erectile dysfunction and pulmonary arterial hypertension (PAH) using **8** (sildenafil, ViagraTM), **9** (vardenafil, LevitraTM), tadalafil (CialisTM), and avanafil (StendraTM) [9,20,32,88–90]. Additionally, an increased myocardial expression of PDE5A in advanced heart failure has been reported [91]. Hence, PDE5A inhibitors are also suggested to prevent or reverse cardiac hypertrophy and adverse cardiac remodeling and to have cardioprotective effects against ischemia or reperfusion injury [9,91–94].

Chekol *et al.* [25,95–97] developed a series of ^{11}C - and ^{18}F -labeled derivatives of specific PDE5A inhibitors known from literature [97–99] for *in vivo* quantification of PDE5A in pulmonary vasculature and visualization of PDE5A expression in myocardium via PET (Figure 3). Most of the PDE5A radioligands have been prepared by *N*-alkylation of the corresponding amine precursors using [^{11}C]methyl trifluoromethanesulfonate or the 2-[^{18}F]fluoroethyl analogue (Schemes 5 and 6 for [^{11}C]12, [^{18}F]13, and [^{11}C]16). In the case of [^{11}C]11, radiolabeling has been performed by esterification starting

from a carboxylic acid precursor [97]. The retention of these radiolabeled derivatives in lung, which is the tissue with most abundant PDE5A expression [34,87,89], has been the main criterion for their suitability as radioligands for PET imaging of this enzyme [97].

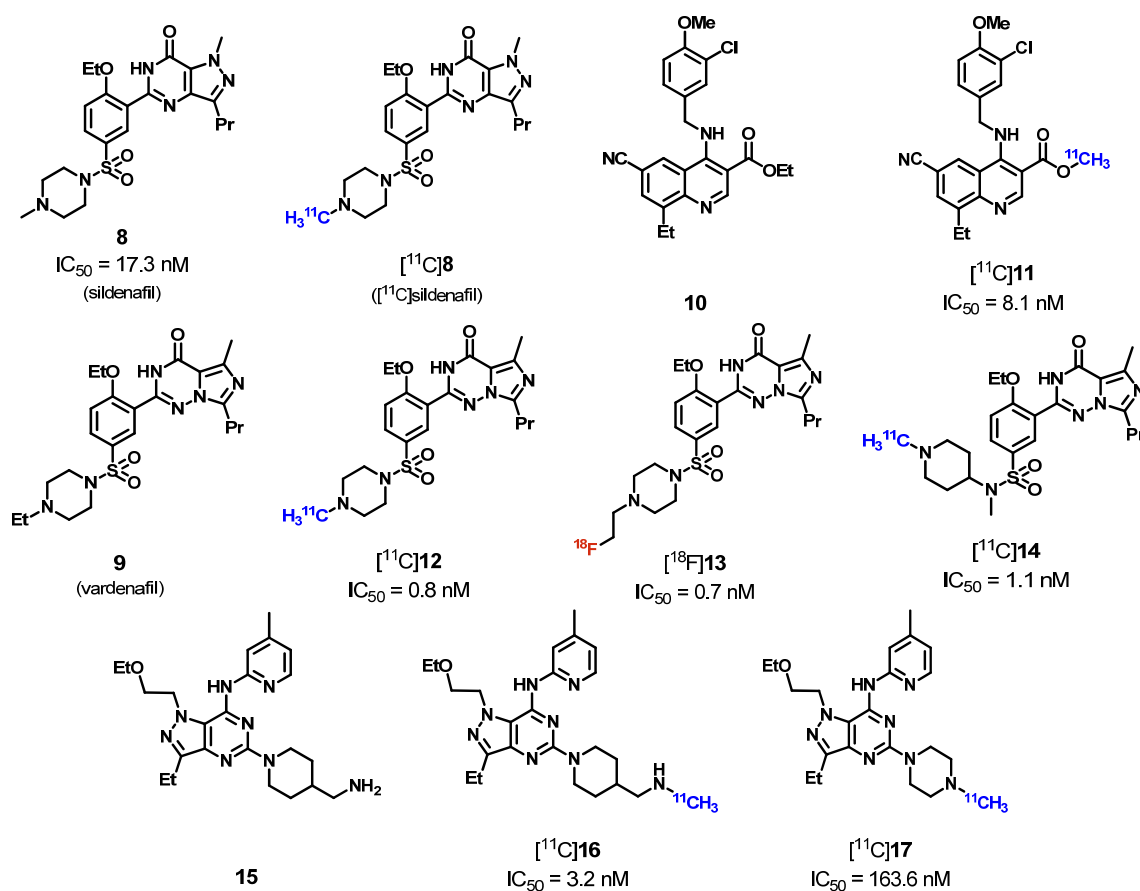


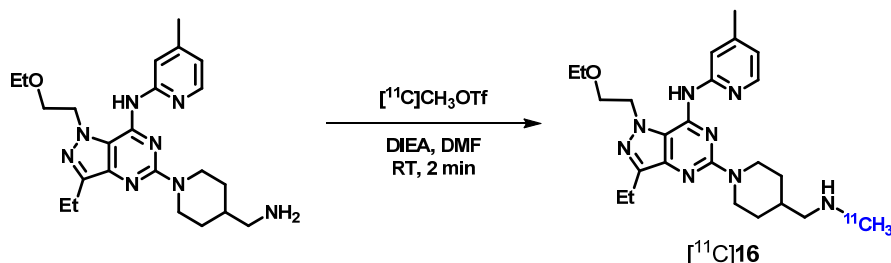
Figure 3. Molecular structures of PDE5A inhibitors and ^{11}C - or ^{18}F -labeled derivatives thereof for PET.



Scheme 5. Radiosyntheses of $[^{11}C]$ 12 and $[^{18}F]$ 13.

In biodistribution studies in mice, low accumulation in lung has been observed for the ^{11}C -labeled sildenafil $[^{11}C]$ 8, the 4-benzylaminoquinoline derivative $[^{11}C]$ 11, and the ethoxyethyl pyrazolopyrimidine-based $[^{11}C]$ 17 followed by high to moderate uptake of $[^{11}C]$ 16 and the radiolabeled vardenafil derivative $[^{11}C]$ 14 [97]. Out of this series, the most potent derivatives $[^{11}C]$ 12 and $[^{18}F]$ 13 displayed the highest accumulation in lung with standard uptake values (SUVs) of 8.0 and 8.9, respectively, at 30 min post injection [97]. Furthermore, $[^{11}C]$ 12 showed a 40-fold increased uptake in heart of transgenic mice overexpressing cardiac specific PDE5 [25,95]. Blocking studies have been performed for $[^{11}C]$ 12 and $[^{11}C]$ 16 using the specific PDE5A inhibitor tadalafil at which accumulation

of the radioligands in lung could be reduced significantly (SUV = 8.0 vs. 1.0 and 6.6 vs. 3.6) [97]. In conclusion, the radiolabeled vardenafil derivatives [^{11}C]12 and [^{18}F]13 as well as compound [^{11}C]16 are recommended as appropriate radioligands for *in vivo* imaging of PDE5A protein and thus have been selected for further biological investigation by the authors [97].

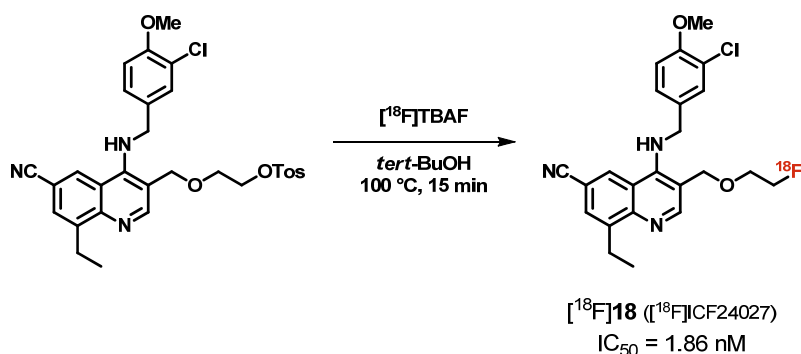


Scheme 6. Radiosynthesis of [^{11}C]16.

Besides the pharmacological interest of inhibiting PDE5A activity in peripheral disorders, expression of this enzyme in specific brain regions like cerebellum, hippocampus, substantia nigra, medulla, and thalamus indicate an important role of PDE5A in the central nervous system associated with neuroinflammatory and neurodegenerative processes as well as cognition [34,100–102]. It has been demonstrated that PDE5 inhibitors have neuroprotective effects in different animal models of neurological diseases [103–106]. In particular, benefits of **8** (sildenafil) in cognition deficits have been observed in transgenic mouse models of Alzheimer's disease [107,108]. However, it was unclear whether **8** readily crosses the blood-brain barrier [109]. With regard to that, PET studies with [^{11}C]8 in rats have been performed [109], but this radioligand displayed low brain uptake (SUV = 0.18 at 30 min p.i.), homogenous distribution and negligible specific binding as a result of metabolic degradation probably caused by *N*-dealkylation and formation of [^{11}C]CH₃OH. However, quantification of **8** and cGMP levels in the cerebrospinal fluid of non-human primates clearly proved that this PDE5 inhibitor is brain penetrating after oral administration at a therapeutic dose suggesting its indication for treatment of Alzheimer's disease [109].

Up to now, no successful detection of PDE5 in the brain for quantification of its expression or occupancy has been reported. Very recently, the ^{18}F -labeled quinoline-based radioligand [^{18}F]18 ([^{18}F]IC24027, Scheme 7) for PET imaging of PDE5A in the brain has been developed by researchers from the Institut national de la santé et de la recherche médicale (INSERM), Clermont-Ferrand, France, in cooperation with our group [110]. Radiosynthesis of [^{18}F]18 has been performed by nucleophilic aliphatic substitution of the tosylate group of the corresponding precursor using tetra-*n*-butylammonium [^{18}F]fluoride in *tert*-butanol (Scheme 7).

In vitro autoradiographic studies on porcine brain slices revealed highest binding densities of [^{18}F]18 in the substantia nigra followed by corpus callosum which is consistent with the known PDE5A distribution pattern in human brain tissue [111]. However, [^{18}F]18 binding was only slightly reduced by co-incubation with the non-radioactive reference compound and **8** (sildenafil) indicating a moderate specific binding of this radioligand. That may be a result of the low PDE5 expression in the brain with only nanomolar density [112] and therefore, a radioligand with subnanomolar PDE5 potency is needed for quantification of this enzyme in brain. *In vivo* metabolism studies in mice showed fast degradation of [^{18}F]18 with only 7% of intact radioligand in plasma and 12%–15% in brain at 30 min post injection, respectively. Two brain penetrating radiometabolites have been observed [110]. In conclusion, [^{18}F]18 is not suitable for PET neuroimaging of PDE5 because of the insufficient specificity of binding and the low metabolic stability. Nevertheless, this outcome will be helpful for our ongoing work in the development of appropriate ^{18}F -labeled quinoline derivatives for visualization and quantification of the PDE5 enzyme in brain with PET.



Scheme 7. Molecular structure and radiosynthesis of $[^{18}\text{F}]\mathbf{18}$ as PDE5A radioligand for PET (TBAF = tetra-*n*-butylammonium fluoride).

5. PDE7 Radioligands

Phosphodiesterase 7 (PDE7) is a cAMP-specific enzyme encoded by the two genes *PDE7A* and *PDE7B*, and is expressed in three cytosolic isoforms [9,20,34] that differ in their coding sequences for the C- and N-terminus. In contrast to other PDE isoforms, the N-termini of *PDE7A* and *PDE7B* are of unknown function and do not contain any of the regulatory subunits so far identified in PDEs [9,20,35]. *PDE7A* is expressed at low levels in the brain and at high levels in spleen, heart, skeletal muscle and several immune cells, for example T lymphocytes [113]. By contrast, *PDE7B* is dominant in the central nervous system with most abundant expression in striatal brain regions such as caudate nucleus, caudate putamen, and nucleus accumbens followed by cortical tissues and hippocampus while in the periphery the highest *PDE7B* levels are found in bladder and heart [9,33–35,114,115].

On the basis of these expression patterns, specific PDE7 inhibitors are suggested as promising approach for treatment of inflammatory and neurological disorders associated with T-cell activation and function [116], Parkinson's disease [117], and addiction [118–120]. However, very little is known about the physiological effects of PDE7 activity to date. With regard to elucidation of the role of this enzyme in several neurological diseases, appropriate PET radioligands would enable *in vivo* imaging and quantification of the PDE7 protein in brain.

In 2015, Thomae *et al.* [121,122] reported on the development of the first two radiolabeled derivatives for that purpose, $[^{18}\text{F}]\mathbf{20}$ ($[^{18}\text{F}]\text{MICA-003}$) and $[^{11}\text{C}]\mathbf{21}$ ($[^{11}\text{C}]\text{MICA-005}$), based on a series of spiroquinazolinones as potent dual PDE7A/B inhibitors, like compound **19** [123] (Figure 4).

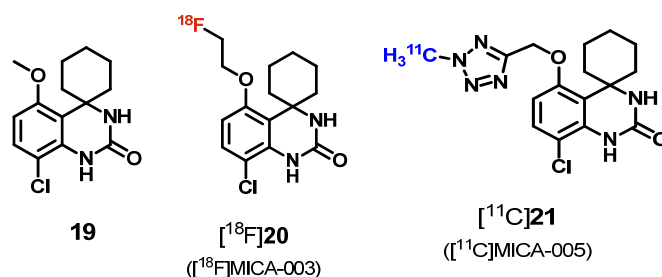
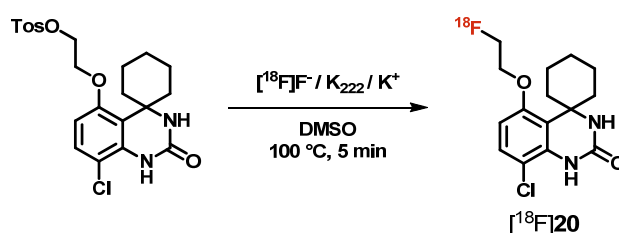


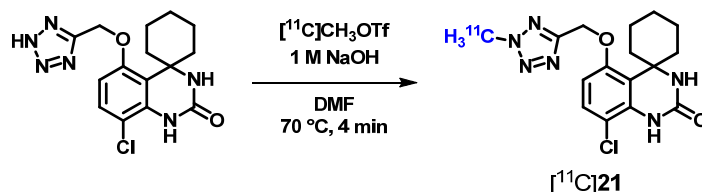
Figure 4. Molecular structures of PDE7A/B inhibitor **19** and ^{18}F - or ^{11}C -labeled derivatives thereof for PET.

The spirocyclic compounds **20** and **21** are of high inhibitory potencies towards PDE7 with IC_{50} values of 17.0 nM and 1.7 nM, respectively [121,122]. The ^{18}F -labeled analogue $[^{18}\text{F}]\mathbf{20}$ has been prepared by nucleophilic aliphatic substitution of the tosylate group of the corresponding precursor using $\text{K}^+ / [^{18}\text{F}]\text{F}^- / \text{K}_{2,2,2}$ -carbonate complex (Scheme 8). A two-step procedure has been performed for the radiosynthesis of $[^{11}\text{C}]\mathbf{21}$ by methylation of the tetrazole precursor with $[^{11}\text{C}]\text{methyl triflate}$

under basic conditions (Scheme 9) [121,122]. Biodistribution studies with [^{18}F]20 in mice revealed a high brain uptake (4%–5%ID/g) at 5 min post injection besides the highest accumulation of this radioligand in heart (10%–11%ID/g) [122]. In microPET imaging studies with [^{18}F]20 and [^{11}C]21, both radioligands displayed rapid uptake and homogenous distribution in the mouse brain followed by a fast wash out [121,122]. For [^{18}F]20 the SUV in brain reached a plateau after 27 min [122] and that, together with the observed non-specific distribution of the radioligands, has been suggested as a result of radiometabolite accumulation in the brain. This presumption has been confirmed by *in vivo* metabolite analysis demonstrating only 74% and 85% of intact [^{18}F]20 and [^{11}C]21 in mouse brain at 5 min post injection, respectively [121,122]. For [^{18}F]20, the brain penetrating radiometabolite has been identified as 2- [^{18}F]fluoroethanol by HPLC analysis using the non-radioactive 2-fluoroethanol as reference [122]. Finally, the radioligands [^{18}F]20 and [^{11}C]21 are suggested to be unfavorable for *in vivo* quantification of PDE7 in the brain via PET, and development of more stable spiroquinazolinone derivatives is currently in progress [122].



Scheme 8. Radiosynthesis of [^{18}F]20.



Scheme 9. Radiosynthesis of [^{11}C]21.

6. PDE10 Radioligands

The dual-substrate specific phosphodiesterase 10 (PDE10) degrades both cAMP and cGMP [124]. The enzyme is encoded by the gene *PDE10A* and expressed in 18 splice variants with cytosolic PDE10A1 and membrane-associated PDE10A2 as the major isoforms in humans [125–127]. Allosteric binding of cAMP activates the enzyme resulting in an increased cAMP degradation at competitive inhibition of cGMP hydrolysis [128,129]. The expression of PDE10A is distinctive and most abundant in striatal brain areas, in particular in medium spiny neurons, with highest levels in caudate nucleus and nucleus accumbens, and at much lower levels in other brain regions [124,130,131]. In peripheral tissues, PDE10A is expressed in testes and to a lower extent for example in the thyroid gland, kidneys, heart, and lung [124,131]. Due to the high PDE10A density in striatum, this enzyme is suggested to play an important role in the pathophysiology of neurodegenerative and neuropsychiatric disorders such as Huntington's disease, Parkinson's disease, and schizophrenia [132–136]. Thus, PDE10A inhibitors are of great interest for treatment of the mentioned brain disorders as reflected by the large number of compounds developed during the last decade [134,136–138]. With regard to that, it is not surprising that PDE10A specific radioligands are also of growing importance for quantification and visualization of this enzyme *in vivo* using PET.

6.1. Radioligands Structurally Related to the PDE10A Inhibitor MP-10

Based on the highly potent PDE10A inhibitor **22** (MP-10, $IC_{50} = 1.26$ nM [139]; $IC_{50} = 0.37$ nM [140]; $IC_{50} = 0.18$ nM with 100-fold selectivity over other PDEs [141]; $IC_{50} = 0.02$ nM [142]; $IC_{50} = 0.64$ nM [143]) and the radiolabeled analogue, [^{11}C]**22** ([^{11}C]MP-10) [141,144–147], a series of structurally related ^{11}C - and ^{18}F -labeled derivatives have been developed for PET imaging of PDE10A as partly reviewed in 2012 by Andrés *et al.* [25,143,144,148–151] (Figure 5).

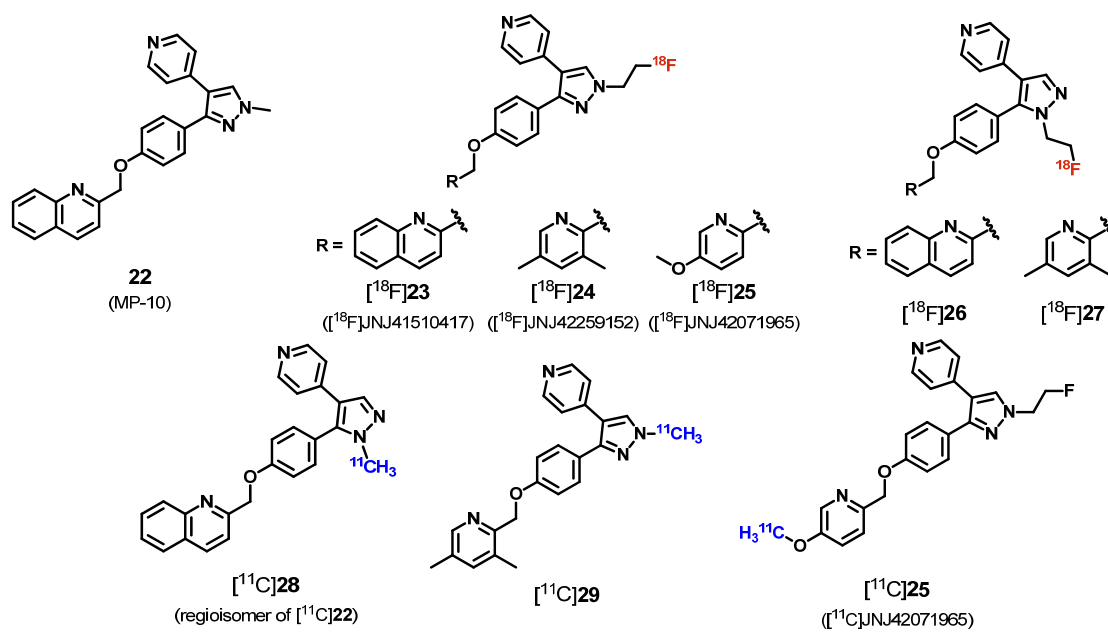


Figure 5. Molecular structures of PDE10A inhibitor **22** and ^{11}C - or ^{18}F -labeled derivatives thereof for PET.

Briefly, in baseline microPET imaging and biodistribution studies in rats and PDE10A knockout mice [^{18}F]**23** (^{18}F JNJ41510417, $IC_{50} = 0.5$ nM [149]) showed PDE10A-specific and reversible binding, but rather slow brain kinetics [25,143,148,149]. The PDE10A radioligands [^{18}F]**24** (^{18}F JNJ42259152, $IC_{50} = 2$ nM [151]; $IC_{50} = 1.58$ nM [143]) and [^{18}F]**25** (^{18}F JNJ42071965, $IC_{50} = 3.16$ nM [143]) are characterized by more favorable kinetic profiles and high striatum-to-cerebellum ratios of 5.4 and 4.4 at 30 min post injection, respectively [143,150,151]. Furthermore, PET studies in healthy humans with [^{18}F]**24** showed appropriate radioligand distribution, brain kinetics, and safety [152,153], and thus, this radioligand has been further evaluated in patients with Huntington's disease (HD) [154]. In this exploratory study, a significant loss of striatal PDE10A levels compared to healthy controls has been observed [154]. Additionally, PET studies with [^{18}F]**24** in a mouse model of HD provided evidence for early regional dysfunctions in PDE10A signaling, involving the caudate putamen and lateral globus pallidus [155]. Moreover, the suitability of [^{18}F]**24** PET for assessment of the pharmacological interaction of dopamine neurotransmission and PDE10A availability in rats has been reported very recently [156].

Notably, [^{18}F]**23**, [^{18}F]**24**, and [^{18}F]**25** all undergo (1) oxidative metabolic cleavage of the phenolic ether bond, as also described for [^{11}C]**22** [141,147], and (2) *N*-dealkylation at the pyrazolo site. This degradation results in the formation of two brain penetrating radiometabolites: (1) the related phenol [141] and (2) 2- ^{18}F fluoroethanol or its oxidation products [25,143,149–151,153]. Despite this, it has been stated that PDE10A can be reliably quantified in the human brain by PET using [^{18}F]**24** [153].

In 2014, Ooms *et al.* [143] published a comparative biological study of several derivatives which are structurally based on the above mentioned radioligands (Figure 5). Radiosyntheses of [^{18}F]**26**

and [^{18}F]27, [^{11}C]28, [^{11}C]29, and [^{11}C]25 have been performed by using [^{18}F]fluoroethyl bromide and [^{11}C]methyl iodide or triflate in dimethylformamide at 90 °C under basic conditions [25,143,150]. Baseline microPET imaging in rats with [^{18}F]26, [^{18}F]27, and [^{11}C]29 revealed no specific accumulation in striatum due to low PDE10A potency [143,150]. In comparison to that, the radioligand [^{11}C]28 ($\text{IC}_{50} = 3.47 \text{ nM}$ [143]) showed slightly higher striatal uptake, but blocking studies in rats and PET imaging in PDE10A knockout mice displayed off target binding in the brain [143]. Finally, [^{11}C]25 exhibited the most favorable brain kinetics as well as the highest specific accumulation in striatum within this series of radioligands structurally related to compound 22 [143]. However, detection of brain penetrating radiometabolites with up to 12% of total activity in cerebellum at 30 min post injection [143] might limit the application of [^{11}C]25, especially for *in vivo* quantification of PDE10A in the brain via PET.

Recently, Fan *et al.* [157] and Li *et al.* [158] reported on the development of further ^{11}C - and ^{18}F -labeled derivatives (Figure 6) out of a small library of pyrazolo-*N*-methyl regioisomers of compound 22 (MP-10) with different substitution patterns at the 2-methylquinoline moiety [158,159].

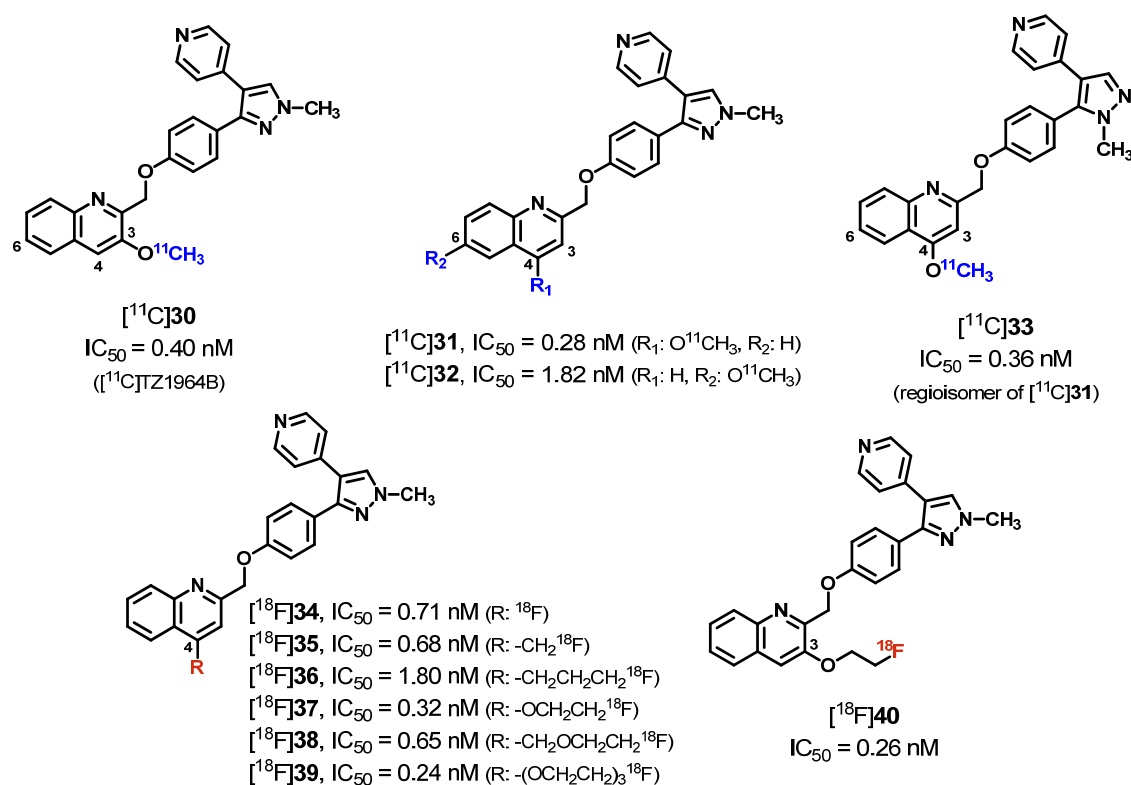
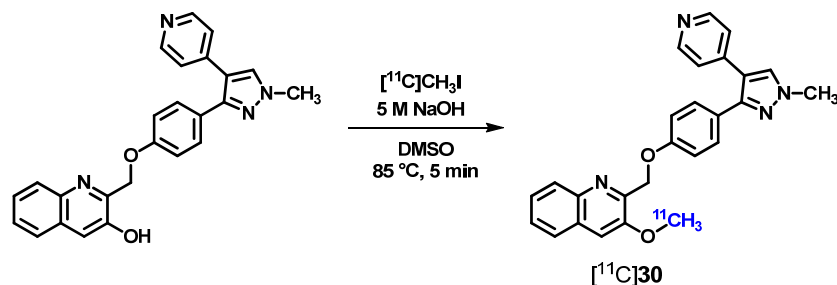


Figure 6. Molecular structures of further ^{11}C - or ^{18}F -labeled derivatives of compound 22 as PDE10A radioligands for PET.

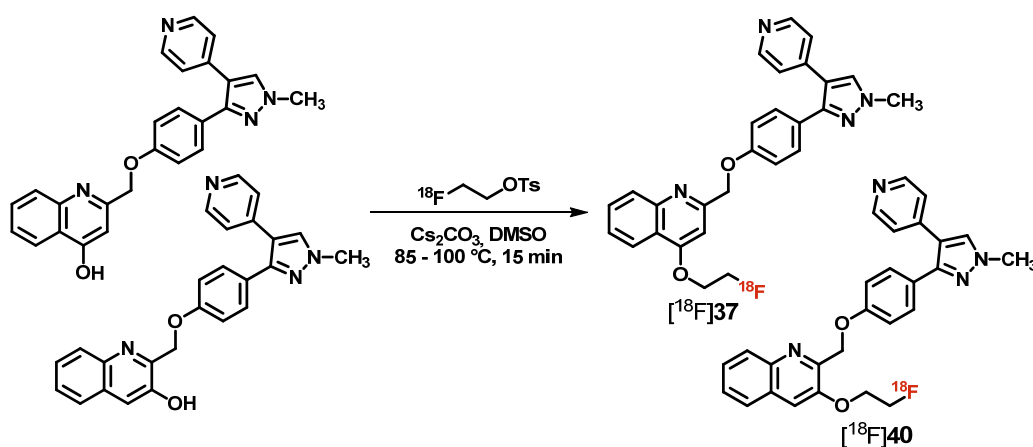
The 3-, 4-, and 6-methoxy derivatives 30 (TZ1964B), 31, and 32 as well as the 4-methoxy regioisomer 33 are of high potency (Figure 6) and selectivity towards PDE10A [157,159]. The radioligands [^{11}C]30–33 have been prepared by methylation of the corresponding quinolinol precursors [158] with [^{11}C]methyl iodide under basic conditions [157] (Scheme 10 for [^{11}C]30). Out of this series, [^{11}C]30 and the most potent derivative [^{11}C]31 showed the highest brain uptake in rats with striatum-to-cerebellum ratios of 6.0 and 4.5 at 60 min post injection, respectively [157]. MicroPET studies in non-human primates with [^{11}C]30 and [^{11}C]31 revealed a high and specific accumulation of both radioligands in striatum. Metabolic degradation of [^{11}C]31 occurred significantly faster compared to [^{11}C]30 with 42% and 65% of the intact radioligands in plasma at 60 min post injection [157]. Further evaluation of [^{11}C]30 (^{11}C]TZ1964B) and its tritiated analogue [^3H]30 (^3H]TZ1964B) in rats and

non-human primates [160] revealed high PDE10A-specific and reversible binding. In conclusion, [^{11}C]30 has been stated as the most promising candidate for *in vivo* quantification and visualization of PDE10A in the brain via PET because of its high brain uptake and striatum-to-cerebellum ratio, good striatal retention, favorable metabolic stability as well as advantageous brain kinetics [157].



Scheme 10. Radiosynthesis of [^{11}C]30.

Out of a series of related fluorine-containing quinoline derivatives, 34–40 (Figure 6) displayed high potency and selectivity towards PDE10A with IC_{50} -values in a range of 0.24 to 1.80 nM [158]. Most of the corresponding radioligands have been prepared in one-step labeling procedures by (1) direct nucleophilic halogen exchange for [^{18}F]34 and [^{18}F]35, and (2) aliphatic substitution via the related tosylate or mesylate precursors for [^{18}F]36, [^{18}F]38, and [^{18}F]39. A two-step labeling strategy has been performed for the radiosyntheses of [^{18}F]37 and [^{18}F]40 using 2-[^{18}F]fluoroethyl tosylate [158] (Scheme 11).



Scheme 11. Radiosyntheses of [^{18}F]37 and [^{18}F]40.

In biodistribution studies in rats, all of these radioligands showed comparable or even higher brain uptake than [^{11}C]22 ([^{11}C]MP-10). However, [^{18}F]34–36 have failed due to an increasing accumulation of activity in bone during the 60-min scan indicating metabolic defluorination of these radioligands. The 4- or 3-fluoroethoxy derivatives [^{18}F]37 and [^{18}F]40 have been identified as the most promising radioligands based on ≥ 2 -fold striatum-to-non-target (cerebellum or cortex) ratios at 30 min post injection, fast clearance from non-target regions and specific binding in the PDE10A-enriched striatum [158]. Thus, [^{18}F]37 and [^{18}F]40 have been further evaluated in non-human primates. MicroPET imaging studies displayed high accumulation of both radioligands in caudate and putamen with striatum-to-non-target ratios > 3 at 40 min post injection as well as enhanced washout kinetics over [^{11}C]22 [158]. Metabolism studies at 30 min post injection revealed $> 90\%$ and 73% of intact [^{18}F]37 or [^{18}F]40 in plasma while two polar radiometabolites for each radioligand have been detected,

and further validation of [^{18}F]37 and [^{18}F]40 is in progress to clarify the suitability of these derivatives for PET imaging of PDE10A in the brain [158].

In 2015, Hamaguchi *et al.* [161] reported on the development of another series of compound 22-related derivatives based on the quinoline analogue 41 [162] (Figure 7). Compared to 22 (MP-10), compound 41 is of reduced inhibitory potency towards PDE10A ($\text{IC}_{50} = 29 \text{ nM}$ vs. 0.55 nM [161,162]), but of higher metabolic stability as shown by *in vitro* studies using mouse and human liver microsomes (M/HLM) [162]. Structural modification of 41 led to the most promising derivative 42 that exhibited a significantly increased PDE10A potency ($\text{IC}_{50} = 5.1 \text{ nM}$) and further enhanced *in vitro* stability in M/HLM studies [161]. Thus, 42 has been selected for ^{11}C -labeling to evaluate this novel PDE10A inhibitor *in vivo* with PET (Figure 7).

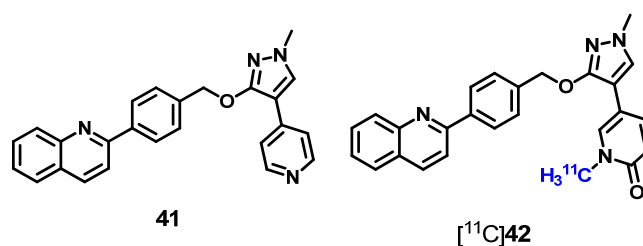
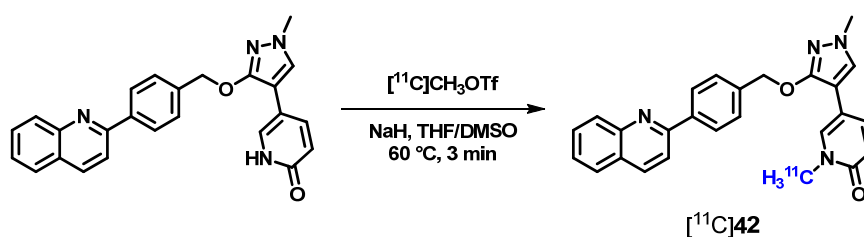


Figure 7. Molecular structures of PDE10A inhibitor 41 and the ^{11}C -labeled derivative thereof for PET.

The radioligand [^{11}C]42 has been prepared by methylation of the corresponding pyridinone precursor using [^{11}C]methyl triflate under basic conditions [161] (Scheme 12). Biodistribution studies in mice revealed a significantly higher accumulation of [^{11}C]42 in striatum than in cerebellum with SUVs of 0.6 and 0.2 at 60 min post injection, respectively [161]. PET imaging studies in rats displayed specific uptake of [^{11}C]42 in striatum that could be blocked after pre-treatment with an excess of 22 (10 mg/kg). Hence, [^{11}C]42 has been stated to show good brain penetration and high specificity of binding in rodents [161]. These preliminary results indicate the suitability of [^{11}C]42 for PET imaging of PDE10A in the brain. However, further data concerning *in vivo* metabolism studies and dosimetry have not been published yet.



Scheme 12. Radiosynthesis of [^{11}C]42.

6.2. Radioligands Structurally not Derived from the PDE10A Inhibitor MP-10

To possibly overcome the problem of metabolic stability of derivatives related to the scaffold of compound 22 (MP-10), our group generated the structurally different radioligand [^{18}F]45 [163,164] (Figure 8) for PET imaging of PDE10A that has already been mentioned by Andrés *et al.* [25]. Based on the potent papaverine-related PDE10A inhibitor 44 (PQ-10, $K_i = 4 \text{ nM}$ [165]; $\text{IC}_{50} = 16 \text{ nM}$ [166]) published by Pfizer [165] (Figure 8), the novel corresponding ^{18}F -labeled fluoroethyl derivative [^{18}F]45 has been developed [164,166].

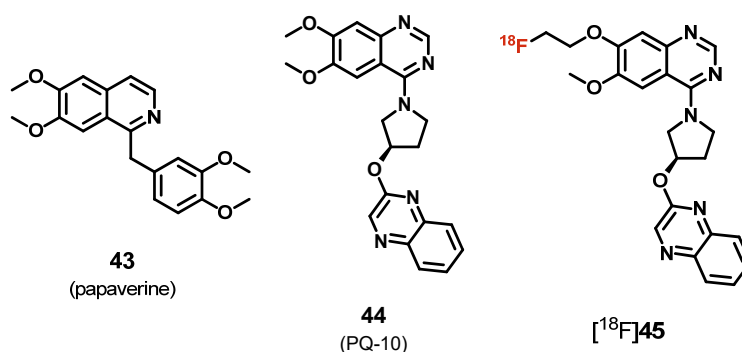


Figure 8. Molecular structures of **43**, a related PDE10A inhibitor and the ^{18}F -labeled derivative thereof for PET.

In vitro autoradiography on rat brain slices displayed region-specific binding of $[^{18}\text{F}]45$ which corresponds with the distribution pattern of PDE10A in rat brain [130]. However, non-displaceable binding of $[^{18}\text{F}]45$ in particular brain regions of known PDE3A expression [167] has been observed. Therefore, it is assumed that $[^{18}\text{F}]45$ additionally binds to PDE3A as indicated by the non-negligible inhibitory potency of this radioligand towards PDE3A ($\text{IC}_{50} = 88.7 \text{ nM}$ [168]) [164]. Biodistribution studies in mice displayed insufficient brain uptake as well as low specific binding of $[^{18}\text{F}]45$. Metabolism studies revealed 70% of intact $[^{18}\text{F}]45$ in mouse plasma at 60 min post injection whereas a single lipophilic radiometabolite has been detected [164]. In the brain, a very high fraction of intact $[^{18}\text{F}]45$ has been observed with 94% and 93% at 30 and 60 min post injection, respectively. In conclusion, $[^{18}\text{F}]45$ has been stated to be unsuitable for quantitative PET imaging of PDE10A due to its low specificity [164].

Consequently, further development of appropriate PDE10A radioligands in our group was based on an alternative structural approach using 1-arylimidazo[1,5-*a*]quinoxaline **46** (Figure 9) as lead compound [169]. Out of a small library of 1- and 8-(2'-fluoro)pyridine-substituted derivatives of **46** [170,171], compound **47** (AQ28A, Figure 9) showed high potency as well as best selectivity towards PDE10A ($\text{IC}_{50} = 2.95 \text{ nM}$ and $> 1000 \text{ nM}$ for all other PDEs [171]) and has been selected for ^{18}F -labeling [170,172,173].

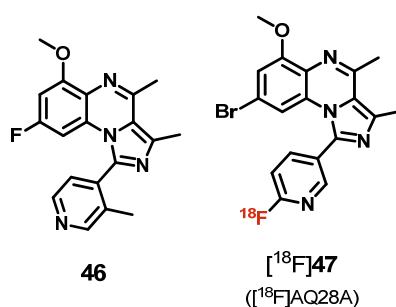
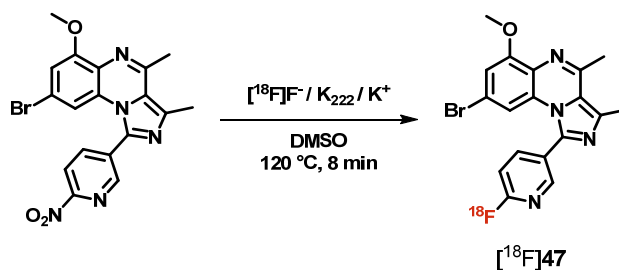


Figure 9. Molecular structures of a PDE10A inhibitor and the ^{18}F -labeled derivative thereof for PET.

$[^{18}\text{F}]47$ has been prepared initially by direct nucleophilic halogen exchange using the related bromo precursor and the $\text{K}^+ / [^{18}\text{F}]\text{F}^- / \text{K}_{2,2,2}$ -carbonate complex in dimethyl sulfoxide [170,173]. To increase the radiochemical yield of $[^{18}\text{F}]47$, an optimized nucleophilic aromatic radiosynthesis procedure starting from the corresponding nitro precursor has been developed [172,173] (Scheme 13). *In vitro* autoradiography on mouse, rat and pig brain slices displayed region-specific binding of $[^{18}\text{F}]47$ [172,173], which corresponds to the known PDE10A distribution pattern in brain of various mammalian species [130,131] and could also be detected by *ex vivo* autoradiographic studies in mouse brain at 30 min post injection. In microPET imaging studies in mice, a high initial brain uptake has

been observed (SUV = 1.8 at 3 min p.i.) with peak accumulation of [^{18}F]47 in striatum (SUV = 2.7 at 4 min p.i.) followed by a fast wash out. Additionally, a striatum-to-cerebellum ratio of 1.4 at 30 min post injection and a 60% reduced striatal uptake after pre-treatment with 22 indicate specific binding of [^{18}F]47 *in vivo*. Metabolism studies in mice revealed 35%–57% of intact [^{18}F]47 in plasma and 71% in brain, respectively, at 30 min post injection [173]. Formation of two brain penetrating radiometabolites has been observed which are slightly more polar than [^{18}F]47 and thus might result from metabolic hydroxylation or *O*-demethylation [169]. However, *in vivo* blocking studies and *ex vivo* autoradiography revealed no specific binding of these radiometabolites either to target- or to non-target regions [173]. Therefore, [^{18}F]47 might be appropriate for quantification of PDE10A in the brain.



Scheme 13. Radiosynthesis of [^{18}F]47.

Notably, although there is evidence that PDE10A is involved in the regulation of whole body energy balance [174], to the best of our knowledge, PDE10A expression associated with obesity has not been analyzed so far. Hence, we used [^{18}F]47 in PET/MR studies in various mouse models of obesity with the aim to quantify PDE10A not only in striatum but also in brown adipose tissue (BAT) [172]. In brief, follow-up studies after high fat diet revealed significantly increased uptake of [^{18}F]47 in BAT and striatum with 130% and 30% higher SUVs compared to controls, respectively [172]. Based on these preliminary results we hypothesize that PDE10A might be a novel therapeutic target for treatment of obesity [172]. Nevertheless, further biological evaluation is needed and currently in progress to verify the suitability of [^{18}F]47 as specific PDE10A imaging agent for PET.

From 2012 to 2015, further ^{11}C - and ^{18}F -labeled radioligands for PET imaging of PDE10A that are structurally different from compound 22 (MP-10) have been reported by several groups and will be discussed in the following section.

The radioligands published by Barret *et al.* [175,176], [^{18}F]48 and [^{18}F]49 ([^{18}F]MNI-654 and [^{18}F]MNI-659, Figure 10), are of high PDE10A binding affinity with K_D -values of 0.029 nM and 0.097 nM [176], respectively.

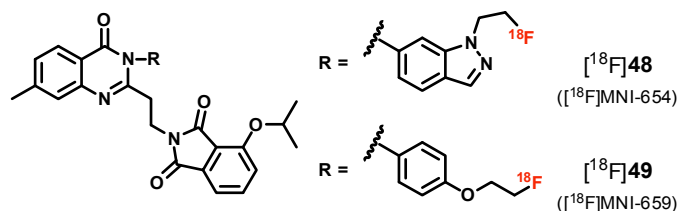
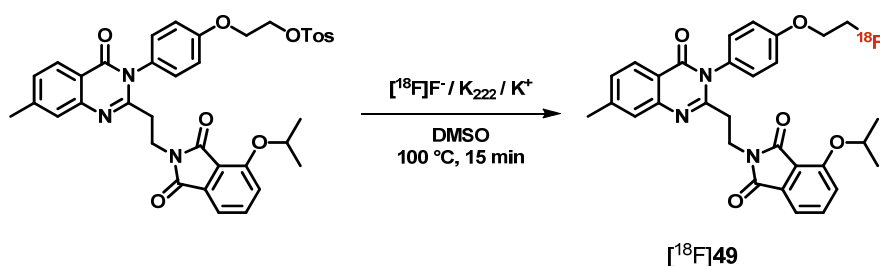


Figure 10. Molecular structures of ^{18}F -labeled PDE10A radioligands for PET.

[^{18}F]48 and [^{18}F]49 have been prepared by nucleophilic aliphatic substitution of the tosylate group of the corresponding precursors using the $\text{K}^+ / [^{18}\text{F}]\text{F}^- / \text{K}_{2,2,2}$ -carbonate complex [176] (Scheme 14 for [^{18}F]49). In preliminary PET studies in non-human and human primates, a region-specific brain uptake of both radioligands paralleling the expected PDE10A distribution and a dose-dependent occupancy of PDE10A by blockade with 22 have been observed [175]. Thus, the authors stated that [^{18}F]48 and

[¹⁸F]49 might be suitable for PET imaging of PDE10A in the brain. Subsequent *in vivo* evaluation in healthy humans revealed moderate metabolic stability of both radioligands and a similar degradation profile with about 20% of intact [¹⁸F]48 and [¹⁸F]49 in plasma at 120 min post injection [176]. In brain distribution studies, a high and specific accumulation of both radioligands in the PDE10A-rich regions caudate, putamen, and globus pallidus has been observed. In these brain areas, [¹⁸F]48 and [¹⁸F]49 showed SUVs of 0.7–1.0 and 1.5–2.5, respectively, at 60 min post injection [176], and [¹⁸F]49 displayed a much faster overall washout than [¹⁸F]48. Based on the more favorable brain kinetics and dosimetry of [¹⁸F]49, this radioligand has been selected for further assessment in patients with Huntington’s disease (HD) [177]. Results of this pilot study revealed that PET imaging with [¹⁸F]49 is of high sensitivity and reliability for basal ganglia PDE10A and can clearly detect pathological loss of striatal PDE10A making it a promising biomarker for longitudinal studies in HD [177]. This assumption has been confirmed in a corresponding PET study in patients with pre-manifest and manifest HD (stage 1 and 2) that revealed significantly reduced [¹⁸F]49 uptake in putamen and caudate nucleus compared to healthy controls [178]. In follow-up studies, about one year later, a more reduced striatal uptake of [¹⁸F]49 has been observed in the HD patients indicating further decreased PDE10A levels, especially in the caudate nucleus [178], but evaluation in a larger HD cohort is needed to confirm these findings [178]. Nevertheless, the previous studies clearly demonstrate the suitability of [¹⁸F]49 for imaging and quantification of PDE10A in the brain via PET as well as for assessment of the enzyme occupancy of novel PDE10A inhibitors developed as therapeutics (www.clinicaltrials.gov: NCT02001389).



Scheme 14. Radiosynthesis of [¹⁸F]49.

On the basis of a pyrazolopyrimidine scaffold, Plisson *et al.* [142] reported on the development of three ¹¹C- and one ¹⁸F-labeled derivatives that have been selected based on the inhibitory potencies of the related non-radioactive compounds 50–53 towards PDE10A (Figure 11).

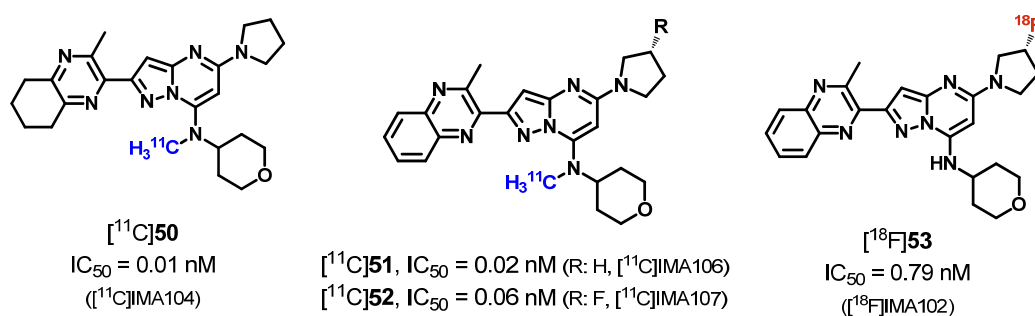
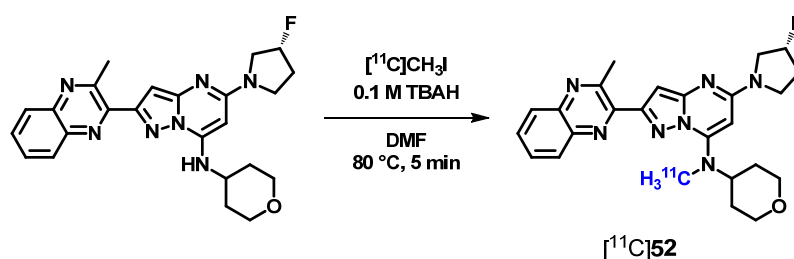


Figure 11. Molecular structures of ¹¹C- or ¹⁸F-labeled PDE10A radioligands for PET.

The radioligands [¹¹C]50 ([¹¹C]JMA104), [¹¹C]51 ([¹¹C]JMA106), and [¹¹C]52 ([¹¹C]JMA107) have been prepared by *N*-alkylation of the corresponding secondary amine precursors with [¹¹C]methyl iodide under basic conditions [142] (Scheme 15 for [¹¹C]52). Radiosynthesis of [¹⁸F]53 ([¹⁸F]JMA102) has been achieved by nucleophilic aliphatic substitution of the mesylate group of the related precursor

using the $K^+ / [^{18}F]F^- / K_{2.2.2}$ -carbonate complex in dimethyl sulfoxide at 120 °C [142]. PET studies in pigs displayed heterogeneous brain distribution of all these radioligands with highest accumulation in striatum. However, the derivative [^{11}C]50 showed slow brain kinetics and [^{18}F]53 exhibited a low striatum-to-rest of brain ratio. Thus, [^{11}C]51 and [^{11}C]52 have been selected for further PET studies in baboons, but in contrast to the previous results in pigs, no washout of [^{11}C]51 from PDE10A-rich brain regions has been observed during the 120-min scan. Also [^{11}C]52 showed similar brain distribution but slightly slower kinetics in baboons than in pigs with peak uptake at 35 min post injection [142]. Both radioligands exhibited comparable moderate metabolic stability with 56% and 50% of intact [^{11}C]51 and [^{11}C]52 in baboon plasma at 90 min post injection [142]. The detected radiometabolites have been stated to be more polar than [^{11}C]51 or [^{11}C]52 and suggested not to be brain penetrating [142].

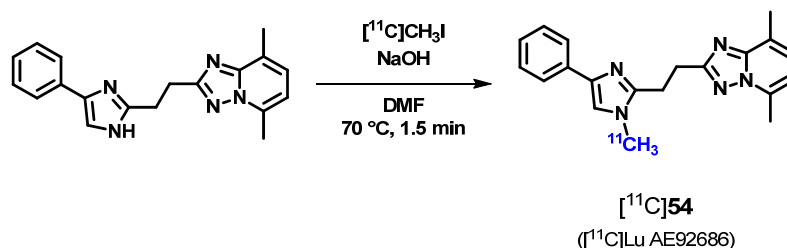


Scheme 15. Radiosynthesis of [^{11}C]52 (TBAH = tetra-*n*-butylammonium hydroxide).

In blocking studies in pigs and baboons, specific binding of [^{11}C]52 in PDE10A-rich brain regions has been confirmed using 53 and compound 22 (MP-10) [142]. Hence, [^{11}C]52 ([^{11}C]IMA107) has been progressed to human PET studies in healthy volunteers [142] resulting in a consistent regional brain distribution and reversible kinetics that indicates a good translation of the radioligand behavior between all species studied. These initial results provided evidence that [^{11}C]52 is appropriate for PET imaging of PDE10A because of good brain penetration, peak uptake in putamen at ~ 25 min (SUV ~ 2.5) and no adverse or clinically detectable pharmacologic effects [142]. In PET studies with [^{11}C]52 in patients with Huntington's disease, an altered PDE10A expression was detectable early before symptomatic onset [179]. This radioligand has also been used to demonstrate striatal and pallidal loss of PDE10A expression, which is associated with duration and severity of motor symptoms and complications in Parkinson's disease [180]. Very recently, further studies with [^{11}C]52 in patients with chronic schizophrenia have been reported [181]. Interestingly, these PET imaging studies revealed no significant differences in [^{11}C]52 uptake in the PDE10A-rich brain regions caudate, putamen, globus pallidus, thalamus, nucleus accumbens, and substantia nigra compared to healthy controls. Hence, the authors concluded that there is no evidence for an altered PDE10A level in patients with schizophrenia [181]. Furthermore, a clinical trial with the PDE10A inhibitor 22 (MP-10) in patients with an acute exacerbation of schizophrenia (www.clinicaltrials.gov: NCT01175135) revealed no differences between subjects that received compound 22 and the placebo control group [181].

These findings clearly show the general importance of PET imaging of PDE10A, and thus of appropriate radioligands for that purpose, to further investigate and understand the complex processes in probably related neuropsychiatric pathologies and the potential of PDE10A inhibitors as therapeutics.

The radioligand [^{11}C]54 ([^{11}C]Lu AE92686, Scheme 16), published by Kehler *et al.* [182,183], has been selected as a promising candidate for PET imaging of PDE10A based on the favorable *in vitro* and *in vivo* properties of the non-radioactive compound [184], such as high inhibitory potency towards PDE10A (IC₅₀ = 0.46 nM [183]; IC₅₀ = 0.32 nM [184]; IC₅₀ = 0.39 nM with > 1000-fold selectivity over other PDEs) and brain uptake (brain-to-plasma ratio in mice = 0.47) [182]. [^{11}C]54 has been prepared by *N*-alkylation of the corresponding imidazole precursor using [^{11}C]methyl iodide under basic conditions [182,183] (Scheme 16).



Scheme 16. Molecular structure and radiosynthesis of $[^{11}\text{C}]\text{54}$ as PDE10A radioligand for PET.

Metabolism studies revealed fast *in vivo* degradation in rats and non-human primates with only 15% and 27% of intact $[^{11}\text{C}]\text{54}$ in plasma at 40 and 30 min post injection, respectively [182]. In rat brain, detection of a small amount of polar radiometabolites has been reported. PET studies with $[^{11}\text{C}]\text{54}$ in non-human primates displayed rapid brain uptake with highest accumulation in striatum and a fast overall wash out indicating a favorable kinetic profile. Specificity of $[^{11}\text{C}]\text{54}$ binding has been confirmed by pre-treatment with compound **22** (MP-10) resulting in a considerably dose-dependent decrease in striatal uptake [182]. Further evaluation of $[^{11}\text{C}]\text{54}$ in human PET studies revealed a comparable brain distribution with peak uptake in striatum at 40 min post injection (SUV ~ 4) that slowly decreased afterwards. Notably, a significantly slower metabolism with about 70% of intact radioligand in plasma at 60 min post injection was observed [182]. In conclusion, $[^{11}\text{C}]\text{54}$ seems to be suitable for PET imaging and quantification of PDE10A in the human brain.

Hwang *et al.* [185–187] reported on the development of $[^{11}\text{C}]\text{55}$ and $[^{18}\text{F}]\text{56}$ ($[^{11}\text{C}]\text{AMG 7980}$ and $[^{18}\text{F}]\text{AMG 580}$, Figure 12) which have been selected as potential PET radioligands because of their high inhibitory PDE10A potencies, and in particular $[^{18}\text{F}]\text{56}$ because of its extraordinary selectivity ($\text{IC}_{50} > 30\text{ }\mu\text{M}$ for other PDEs). Furthermore, high to very high binding affinities of the corresponding tritiated analogues towards PDE10A have been estimated with a K_D -value of 0.94 nM for $[^3\text{H}]\text{55}$ in rat striatal homogenate [188] and K_D -values of 51.7 pM, 71.9 pM, and 83.1 pM (male) or 84.1 pM (female) for $[^3\text{H}]\text{56}$ in rat, baboon, and human striatal tissues, respectively [187].

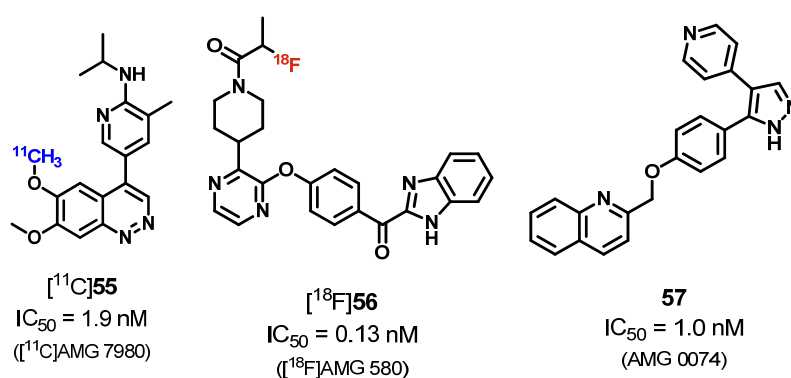
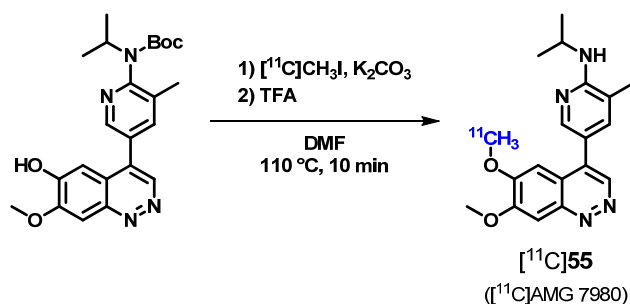
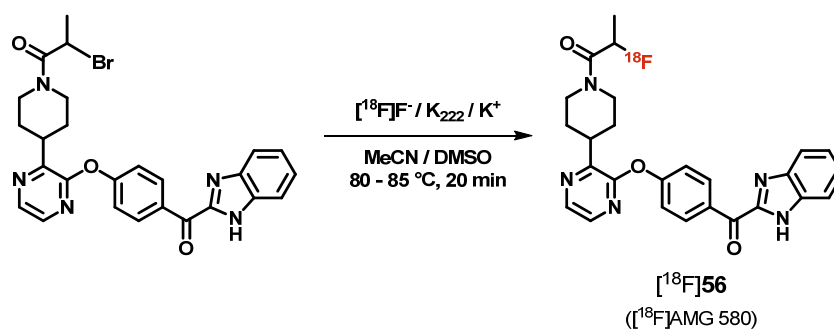


Figure 12. Molecular structures of ^{11}C - or ^{18}F -labeled PDE10A radioligands for PET and the PDE10A inhibitor **57**.

The radioligand $[^{11}\text{C}]\text{55}$ has been prepared in a one-pot two-step radiosynthesis by ^{11}C -labeling of the *N*-*tert*-butoxycarbonyl (BOC)-substituted phenol precursor using $[^{11}\text{C}]\text{methyl iodide}$ followed by acidic hydrolysis to remove the protecting group [185] (Scheme 17). Radiosynthesis of $[^{18}\text{F}]\text{56}$ has been performed by direct nucleophilic aliphatic halogen exchange using the corresponding bromo precursor and the $\text{K}^+ / [^{18}\text{F}]\text{F}^- / \text{K}_{2,2,2}\text{-carbonate}$ complex [187] (Scheme 18).

Scheme 17. Radiosynthesis of $[^{11}\text{C}]\mathbf{55}$.Scheme 18. Radiosynthesis of $[^{18}\text{F}]\mathbf{56}$.

Characterization of $[^{11}\text{C}]\mathbf{55}$ in non-human primates revealed fast metabolism with 33% of intact radioligand in plasma at 30 min post injection. Related PET imaging studies displayed distribution of $[^{11}\text{C}]\mathbf{55}$ throughout the brain with highest accumulation in PDE10A-specific regions like putamen and globus pallidus followed by a fast wash out [185]. The striatal uptake of $[^{11}\text{C}]\mathbf{55}$ decreased in a dose-dependent manner after pre-treatment with a non-specified PDE10A inhibitor indicating moderate specific binding [185]. The authors suggested this might be a result of the fast dissociation rate of $[^{11}\text{C}]\mathbf{55}$ as determined in the *in vitro* binding assay with $[^3\text{H}]\mathbf{55}$ (dissociation half-life = 0.1 min [188]) [186].

By contrast, the related (*R*)- and (*S*)-enantiomers of $\mathbf{56}$ exhibited dissociation half-lives of 3.1 and 0.8 min [187,188]. *In vitro* autoradiography on rat, baboon, and human brain slices displayed a high and specific striatal accumulation of $[^3\text{H}]\mathbf{56}$ that is consistent with the known PDE10A expression pattern [34,130,131] and could be blocked significantly by co-incubation with an excess of the PDE10A inhibitor $\mathbf{57}$ (AMG 0074, Figure 12) [187]. In microPET studies with $[^{18}\text{F}]\mathbf{56}$ in rats, rapid brain penetration and region-specific uptake have been observed with highest accumulation in striatum (SUV = 2.77 at ~ 50 min p.i.), as well as moderate to low uptake in nucleus accumbens (SUV = 0.94) and cerebellum (SUV = 0.58) [187]. Based on these results, $[^{18}\text{F}]\mathbf{56}$ has been further evaluated in non-human primates [186]. Metabolism studies in baboons and rhesus monkeys revealed fast *in vivo* degradation of $[^{18}\text{F}]\mathbf{56}$ with approximately 25% or 35% of intact radioligand in plasma, respectively, at 30 min post injection. Corresponding PET studies displayed high accumulation of $[^{18}\text{F}]\mathbf{56}$ in striatum and low uptake in other brain regions comparable to the previous findings in rats [186]. Specificity of $[^{18}\text{F}]\mathbf{56}$ binding *in vivo* has been confirmed by pre-treatment with compound $\mathbf{22}$ (MP-10), but significantly reduced accumulation in the target regions has been obtained only at a larger excess of $\mathbf{22}$ (3 mg/kg) [186]. Furthermore, the PET images revealed higher levels of whole brain uptake in rhesus monkeys that might indicate higher non-specific binding and/or a slower wash out of $[^{18}\text{F}]\mathbf{56}$ compared to that in baboons.

In conclusion, these *in vivo* studies do not clearly verify whether $[^{11}\text{C}]\mathbf{55}$ or $[^{18}\text{F}]\mathbf{56}$ might be suitable for PET imaging of PDE10A in the brain. Notably, the low metabolic stability observed in

non-human primates could possibly restrict the human application of these radioligands, especially when brain penetrating radiometabolites are formed.

Moreover, a series of ^{11}C -labeled radioligands based on a pyrazolopyridazine scaffold [189] has been reported by Stepanov *et al.* [190]. The radioligands [^{11}C]58–64 (Figure 13) have been prepared by *O*-alkylation of the corresponding 1,3-disubstituted 5-hydroxypyridazin-4(1*H*)-one precursors using [^{11}C]methyl triflate under basic conditions [190] (Scheme 19 for [^{11}C]61).

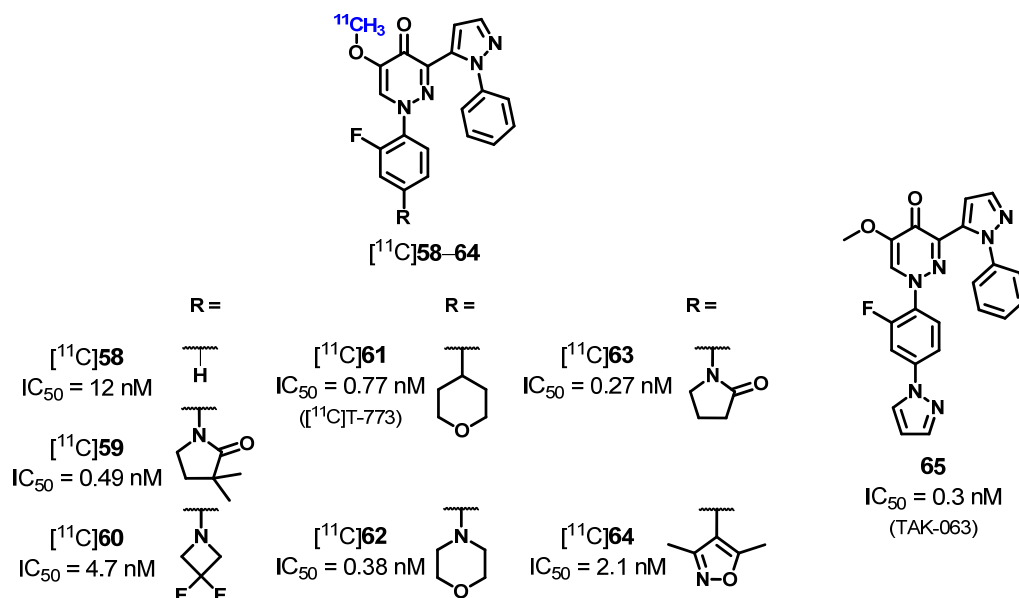
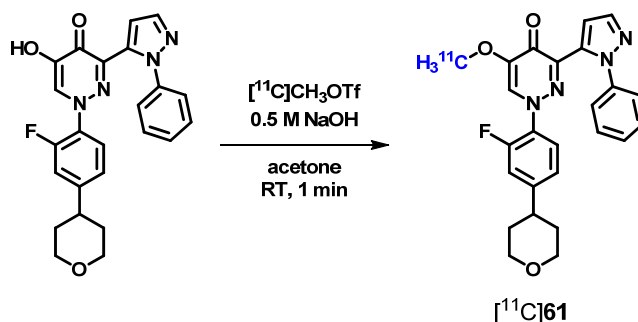


Figure 13. Molecular structures of ^{11}C -labeled PDE10A radioligands for PET and the PDE10A inhibitor 65.



Scheme 19. Radiosynthesis of [^{11}C]61.

Characterization of these radioligands in non-human primates revealed that [^{11}C]58–60 and [^{11}C]62–64 are not suitable for PET imaging of PDE10A in the brain because of low brain uptake, moderate to fast *in vivo* degradation as well as formation of brain penetrating radiometabolites, low specific binding, and unfavorable kinetic profiles [190].

The radioligand [^{11}C]61 ([^{11}C]T-773) has been stated as the most promising derivative out of this series. *In vitro* autoradiography with the tritiated analogue [^3H]61 ([^3H]T-773) on brain sections of mouse displayed region-specific binding in caudate putamen, globus pallidus, nucleus accumbens, and substantia nigra while no accumulation in PDE10A knock-out animals was observed [191]. By co-incubation with various PDE10A inhibitors such as compound 22 (MP-10) and reference 61 (T-773), a considerably decreased accumulation of [^3H]61 in wild-type mouse and rat brain sections indicates high specific binding of this radioligand [191]. Additionally, *in vitro* autoradiography with

[³H]61 and [¹¹C]61 on primate and human brain sections revealed high accumulation in striatum that is comparable to the known expression pattern of PDE10A in monkey and human brain [131] and could be blocked significantly by 22 in both species [191,192].

PET imaging studies in rhesus monkeys with [¹¹C]61 revealed a high brain uptake with peak accumulation in putamen and caudate and lowest uptake in cortical regions, as well as favorable brain kinetics. [¹¹C]61 exhibited a high putamen-to-cerebellum ratio of about 5.3 at 120 min and a mean striatum-to-cerebellum ratio of 5.1 from 87 min to 123 min post injection [190,192]. Metabolism studies revealed moderate stability of [¹¹C]61 with 56% and 45% of the intact radioligand in plasma at 30 min and 90 min post injection [191], respectively, and four radiometabolites which are more polar than [¹¹C]61 [190]. PET-studies with 22 as blocking agent displayed substantial decrease in striatal uptake as well as putamen-to-cerebellum ratio and demonstrated high PDE10A-specific and reversible binding of [¹¹C]61 [192].

Moreover, [¹¹C]61 has been evaluated in PDE10A knock-out and normal mice with PET [193]. These studies showed that [¹¹C]61 is appropriate for *in vivo* quantification of PDE10A in the rodent brain and revealed significantly lower striatal protein levels in knock-out compared to control animals with %SUVs of 48.2 and 63.6 for heterozygous and homozygous knock-out mice, respectively, and 85.1 for wild-type mice between 15 and 63 min post injection [193].

Very recently, [¹¹C]61 has been applied in a PET study [194] investigating the PDE10A brain occupancy by the novel PDE10A inhibitor 65 (TAK-063, Figure 13) in non-human primates [195]. The results additionally provide evidence for the suitability of [¹¹C]61 to evaluate striatal PDE10A levels *in vivo* although unclear interactions of uptake between [¹¹C]61 and 65 in the non-target region cerebellum have been observed (decreased uptake of [¹¹C]61 after pre-treatment with 65) [194].

In conclusion, the favorable brain kinetics, high specificity of binding and preliminary dosimetry results indicate that [¹¹C]61 might be a promising PET radioligand for *in vivo* imaging and quantification of PDE10A in the human brain.

Finally, the radioligands [¹¹C]66–69 (Figure 14), published by Cox and Hostetler *et al.* [196,197], have been selected from Merck high-throughput screening hits mainly on the basis of the high PDE10A-affinity of their non-radioactive analogues as well as > 27,000–100,000-fold selectivity over other PDEs.

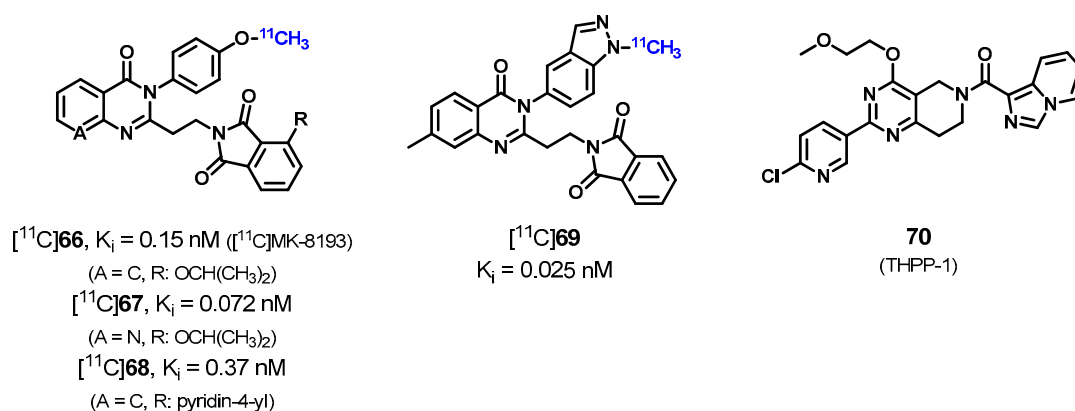
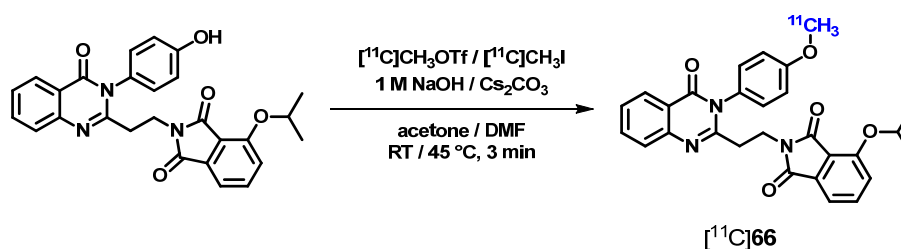


Figure 14. Molecular structures of ¹¹C-labeled PDE10A radioligands for PET and the PDE10A inhibitor 70.

In baseline PET studies in rhesus monkeys, [¹¹C]66 ([¹¹C]MK-8193) showed a high brain uptake with a PDE10A-specific accumulation in striatum followed by a fast wash-out phase. In comparison to [¹¹C]66, the derivative [¹¹C]68 displayed high non-specific binding and a possibly brain penetrating radiometabolite, [¹¹C]67 showed lower specificity of binding, and [¹¹C]69 revealed slower overall elimination [196]. Development of a [¹⁸F]fluoroethyl analogue of [¹¹C]66 and *in vivo* evaluation of this radioligand has also been mentioned briefly without any related data published so far. Besides,

further ^{11}C -labeled analogues of the selective PDE10A inhibitor **70** (THPP-1, Figure 14) [198] have been studied *in vivo* that uniformly displayed poor brain uptake as also shortly reported in this article [196].

Consequently, the authors stated [^{11}C]**66** to be the most promising candidate out of this series because of its favorable *in vivo* profile including brain uptake and kinetics, as well as an appropriate target-to-non-target ratio indicating high specific binding [196]. Radiosynthesis of [^{11}C]**66** has been performed by *O*-alkylation of the corresponding phenol precursor using [^{11}C]methyl triflate or [^{11}C]methyl iodide under basic conditions [196,197,199] (Scheme 20).



Scheme 20. Radiosynthesis of [^{11}C]**66**.

In vitro autoradiography with the tritiated analogue [^3H]**66** (^3H]MK-8193) on rat, rhesus monkey, and human brain sections displayed high and specific binding in caudate putamen and nucleus accumbens, and moderate to low binding density in hippocampus, cerebellum, brain stem, thalamus, and cerebral cortex for all three species [199]. Binding studies with [^3H]**66** in rat, monkey, and human striatum homogenates revealed K_D -values of 0.11 nM, 0.12 nM, and 0.13 nM, respectively, demonstrating high affinity of this radioligand towards PDE10A [199]. In further PET imaging studies in rhesus monkeys, a rapid and high brain uptake of [^{11}C]**66** has been observed with peak accumulation in striatum at 30 min post injection (SUV \sim 2.4) followed by a fast clearance [199] which is consistent with the results described above. In contrast, PET studies in rats showed lower initial peak uptake in striatum (SUV \sim 0.7) [199]. Blocking studies after pre-treatment with **70** displayed a significantly decreased striatal uptake in both species [199] indicating high specific binding of [^{11}C]**66**. Although no detailed data concerning *in vivo* stability of [^{11}C]**66** have been published yet, there is no evidence for brain penetrating radiometabolites [199]. Based on these preliminary findings, [^{11}C]**66** (^{11}C]MK-8193) appears to be a suitable radioligand for PET imaging of PDE10A in the brain.

Overall, 35 novel PDE10A radioligands have been published since 2012 indicating the great interest in this enzyme as an important target in the diagnosis and treatment of several diseases. Especially for neurodegenerative and neuropsychiatric disorders, further advances in investigating the role of PDE10A were enabled by appropriate imaging agents for PET. For example, clinical PET studies clearly showed a pathological loss of striatal PDE10A in Huntington's disease but indicated that the expression of PDE10A is not altered in schizophrenia leading to a discussion on the involvement of the PDE10A protein in schizophrenia. Furthermore, *in vivo* quantification of PDE10A in pre-clinical PET studies revealed an increase in the availability of this enzyme in both the striatum and the brown adipose tissue in obese mice pointing to an association of PDE10A with obesity. In conclusion, further evaluation of promising radioligands for imaging and quantification of PDE10A by PET will certainly result in new insights related to diverse research fields.

7. Summary and Concluding Remarks

The regulatory role of cyclic nucleotide phosphodiesterases in the intracellular signal transduction cascades initiated by the secondary messengers cAMP and cGMP is the key reason for the extensive development and application of numerous PDE inhibitors as therapeutics and PDE radioligands as imaging agents for PET. Various clinical indications are determined by the variant-specific expression pattern of the PDE isoenzymes within the organism and include both peripheral diseases as well as disorders of the central nervous system.

The main challenges in generating appropriate PDE radioligands are: (1) a high selectivity towards the particular PDE family, especially for PDE-specific detection in tissues expressing different PDE isoforms (e.g., striatal expression of PDE2A and PDE10A in the brain); and (2) a sufficiently high metabolic stability *in vivo* to enable a precise quantification of the respective PDE in the organ, tissue, or brain region under investigation. Furthermore, it is necessary to take into account the differences among species in the PDE isoenzyme-specific expression, distribution pattern, density, and protein structure [9,15] as well as in the metabolism [200] that may cause altered radioligand binding potency and *in vivo* stability. Thus, the radioligand evaluation in humans could lead to unexpected outcomes compared to pre-clinical studies in rodents and monkeys.

Up to now, the development of several ^{11}C - and ^{18}F -labeled PET radioligands for *in vivo* imaging and quantification of the PDEs 1, 2, 4, 5, 7, and especially 10 has been reported as reviewed before by Andrés *et al.* [25] in 2012 and updated herein by 49 novel radioligands (see Table 1).

Table 1. Update of novel radioligands for PET imaging of PDEs 2, 4, 5, 7, and 10 since 2012.

Phosphodiesterase	Radioligands Review Compound No. (Code No. Given)	References
PDE2	^{18}F]1 (^{18}F]B-23)	[48,55]
	^{18}F]2 (^{18}F]PF-05270430)	[48,56–58]
	^{18}F]3, ^{18}F]4, ^{18}F]5 (^{18}F]TA3–5)	[60–62]
PDE4	^{18}F]7 (^{18}F]MNI-617)	[82]
PDE5	^{11}C]8 (^{11}C]sildenafil), ^{18}F]13, ^{11}C]14, ^{11}C]16, ^{11}C]17	[97]
	^{18}F]18 (^{18}F]ICF24027)	[110]
PDE7	^{18}F]20 (^{18}F]MICA-003), ^{11}C]21 (^{11}C]MICA-005)	[121,122]
	Structurally related to compound 22 (MP-10)	
	^{18}F]26, ^{11}C]29	[143]
	^{11}C]30 (^{11}C]TZ1964B), ^{11}C]31–33	[157,160]
	^{18}F]34–40	[158]
	^{11}C]42	[161]
PDE10	Structurally not derived from compound 22 (MP-10)	
	^{18}F]47 (^{18}F]AQ28A)	[170,172]
	^{18}F]48 (^{18}F]MNI-654), ^{18}F]49 (^{18}F]MNI-659)	[175–178]
	^{11}C]50 (^{11}C]IMA104), ^{11}C]51 (^{11}C]IMA106)	[142,181]
	^{11}C]52 (^{11}C]IMA107), ^{18}F]53 (^{18}F]IMA102)	
	^{11}C]54 (^{11}C]Lu AE92686)	[182,183]
	^{11}C]55 (^{11}C]AMG 7980), ^{18}F]56 (^{18}F]AMG 580)	[185–187]
	^{11}C]58–60, ^{11}C]61 (^{11}C]T-773), ^{11}C]62–64	[190–194]
^{11}C]66 (^{11}C]MK-8193), ^{11}C]67–69	[196,197,199]	

To the best of our knowledge, five of the PDE radioligands summarized in Table 1 have already entered first clinical PET studies in humans, namely ^{18}F]2 (^{18}F]PF-05270430) as a PDE2-specific imaging agent as well as the PDE10 radioligands ^{18}F]48 (^{18}F]MNI-654), ^{18}F]49 (^{18}F]MNI-659), ^{11}C]52 (^{11}C]IMA107), and ^{11}C]54 (^{11}C]Lu AE92686) for investigation of these isoenzymes in the brain. Moreover, pre-clinical *in vivo* evaluation provided evidence for additional eight PET radioligands to be promising candidates for visualization and quantification of PDE5 in lung and heart (^{11}C]12, ^{18}F]13, ^{11}C]16), and for neuroimaging of PDE10 (^{11}C]30 (^{11}C]TZ1964B), ^{11}C]66 (^{11}C]MK-8193), ^{18}F]37, ^{18}F]40, ^{18}F]47 (^{18}F]AQ28A)), and further biological characterization is awaited to confirm the suitability of these compounds. Application of the other reported ^{11}C - and ^{18}F -labeled PDE radioligands is hampered due to low metabolic stability, poor specific binding or unfavorable kinetic profiles.

Besides the main focus on the development of PDE10 radioligands since 2010, specific radioligands for the other PDE families gain in importance as reflected by the increasing number of groups working in this field. PDE2 radioligands, for example, may be useful for PET imaging of Alzheimer's

disease as well as of highly proliferative processes associated with certain types of cancer. Regarding PET neuroimaging of PDE4, the observed low tolerability of the PDE4 protein towards structural modifications at the lead scaffold rolipram might be an explanation for the development of only one novel ^{18}F -labeled derivative (^{18}F 7, ^{18}F MNI-617 [82,83]) since the first report by DaSilva *et al.* [23] in 1997. The situation concerning imaging of PDE5 in the brain via PET is comparable. Already 10 years ago, Jacobsen *et al.* [201] published the first radioligand for that purpose. Although there is strong evidence that PDE5 activity is related to neuroinflammatory and neurodegenerative processes as well as cognition, only one further radioligand for neuroimaging of that isoenzyme has been developed very recently by researchers from France and our group (^{18}F 18 (^{18}F ICF24027)) [110]. Finally, in 2015 the first two PET radioligands for imaging of PDE7, ^{18}F 20 (^{18}F MICA-003) and ^{11}C 21 (^{11}C MICA-005), have been reported by Thomae *et al.* [121,122] to investigate the role of this enzyme in various neurological diseases.

In conclusion, all these efforts reflect the growing interest in the development of radiolabeled isoenzyme-specific PDE ligands for diagnostic and companion imaging by PET, and enlightening findings in this area of clinical research can be expected within the next few years.

Acknowledgments: We thank the Helmholtz Association for covering the costs to publish in open access.

Conflicts of Interest: The authors declare no conflict of interest.

References

1. Wahl, R.L.; Wagner, H.N. *Principles and Practice of PET and PET/CT*, 2nd ed.; Wolters Kluwer/Lippincott Williams & Wilkins: Philadelphia, PA, USA, 2009; p. 729.
2. Brust, P.; van den Hoff, J.; Steinbach, J. Development of ^{18}F -labeled radiotracers for neuroreceptor imaging with positron emission tomography. *Neurosci. Bull.* **2014**, *30*, 777–811. [[CrossRef](#)] [[PubMed](#)]
3. Gallamini, A.; Zwarthoed, C.; Borra, A. Positron emission tomography (PET) in oncology. *Cancers* **2014**, *6*, 1821–1889. [[CrossRef](#)] [[PubMed](#)]
4. Tee, S.S.; Keshari, K.R. Novel approaches to imaging tumor metabolism. *Cancer J.* **2015**, *21*, 165–173. [[CrossRef](#)] [[PubMed](#)]
5. Tarkin, J.M.; Joshi, F.R.; Rajani, N.K.; Rudd, J.H. PET imaging of atherosclerosis. *Future Cardiol.* **2015**, *11*, 115–131. [[CrossRef](#)] [[PubMed](#)]
6. Jivraj, N.; Phinikaridou, A.; Shah, A.M.; Botnar, R.M. Molecular imaging of myocardial infarction. *Basic Res. Cardiol.* **2014**, *109*, 397. [[CrossRef](#)] [[PubMed](#)]
7. Mier, W.; Mier, D. Advantages in functional imaging of the brain. *Front. Hum. Neurosci.* **2015**, *9*, 249. [[CrossRef](#)] [[PubMed](#)]
8. Conti, M.; Jin, S.L. The molecular biology of cyclic nucleotide phosphodiesterases. *Prog. Nucleic Acid Res. Mol. Biol.* **1999**, *63*, 1–38. [[PubMed](#)]
9. Bender, A.T.; Beavo, J.A. Cyclic nucleotide phosphodiesterases: Molecular regulation to clinical use. *Pharmacol. Rev.* **2006**, *58*, 488–520. [[CrossRef](#)] [[PubMed](#)]
10. Omori, K.; Kotera, J. Overview of PDEs and their regulation. *Circ. Res.* **2007**, *100*, 309–327. [[CrossRef](#)] [[PubMed](#)]
11. Hardman, J.G.; Robison, G.A.; Sutherland, E.W. Cyclic nucleotides. *Annu. Rev. Physiol.* **1971**, *33*, 311–336. [[CrossRef](#)] [[PubMed](#)]
12. Francis, S.H.; Corbin, J.D. Cyclic nucleotide-dependent protein kinases: Intracellular receptors for cAMP and cGMP action. *Crit. Rev. Clin. Lab. Sci.* **1999**, *36*, 275–328. [[CrossRef](#)] [[PubMed](#)]
13. Bos, J.L. Epac proteins: Multi-purpose cAMP targets. *Trends Biochem. Sci.* **2006**, *31*, 680–686. [[CrossRef](#)] [[PubMed](#)]
14. Beavo, J.A.; Francis, S.H.; Houslay, M.D. *Cyclic Nucleotide Phosphodiesterases in Health and Disease*, 1st ed.; CRC Press: Boca Raton, FL, USA, 2006; p. 728.
15. Francis, S.H.; Blount, M.A.; Corbin, J.D. Mammalian cyclic nucleotide phosphodiesterases: Molecular mechanisms and physiological functions. *Physiol. Rev.* **2011**, *91*, 651–690. [[CrossRef](#)] [[PubMed](#)]
16. Weiss, B.; Hait, W.N. Selective cyclic nucleotide phosphodiesterase inhibitors as potential therapeutic agents. *Annu. Rev. Pharmacol. Toxicol.* **1977**, *17*, 441–477. [[CrossRef](#)] [[PubMed](#)]

17. Weishaar, R.E.; Cain, M.H.; Bristol, J.A. A new generation of phosphodiesterase inhibitors: Multiple molecular forms of phosphodiesterase and the potential for drug selectivity. *J. Med. Chem.* **1985**, *28*, 537–545. [[CrossRef](#)] [[PubMed](#)]
18. Schudt, C.; Winder, S.; Eltze, M.; Kilian, U.; Beume, R. Zardaverine: A cyclic AMP specific PDE III/IV inhibitor. *Agents Actions Suppl.* **1991**, *34*, 379–402. [[PubMed](#)]
19. Lugnier, C. Cyclic nucleotide phosphodiesterase (PDE) superfamily: A new target for the development of specific therapeutic agents. *Pharmacol. Ther.* **2006**, *109*, 366–398. [[CrossRef](#)] [[PubMed](#)]
20. Keravis, T.; Lugnier, C. Cyclic nucleotide phosphodiesterase (PDE) isozymes as targets of the intracellular signalling network: Benefits of PDE inhibitors in various diseases and perspectives for future therapeutic developments. *Br. J. Pharmacol.* **2012**, *165*, 1288–1305. [[CrossRef](#)] [[PubMed](#)]
21. Fajardo, A.; Piazza, G.; Tinsley, H. The role of cyclic nucleotide signaling pathways in cancer: Targets for prevention and treatment. *Cancers* **2014**, *6*, 436–458. [[CrossRef](#)] [[PubMed](#)]
22. Wang, Z.-Z.; Zhang, Y.; Zhang, H.-T.; Li, Y.-F. Phosphodiesterase: An interface connecting cognitive deficits to neuropsychiatric and neurodegenerative diseases. *Curr. Pharm. Des.* **2015**, *21*, 303–316. [[CrossRef](#)]
23. DaSilva, J.N.; Valente, C.M.; Wilson, A.A.; Warsh, J.J.; Houle, S. Carbon-11 labeling of the selective inhibitors of phosphodiesterase IV RO20–1724 and rolipram. *J. Label. Comp. Radiopharm.* **1997**, *40*, 678–680.
24. DaSilva, J.N.; Lourenco, C.M.; Meyer, J.H.; Hussey, D.; Potter, W.Z.; Houle, S. Imaging cAMP-specific phosphodiesterase-4 in human brain with R-[¹¹C]rolipram and positron emission tomography. *Eur. J. Nucl. Med. Mol. Imaging* **2002**, *29*, 1680–1683. [[CrossRef](#)] [[PubMed](#)]
25. Andrés, J.I.; De Angelis, M.; Alcazar, J.; Celen, S.; Bormans, G. Recent advances in positron emission tomography (PET) radiotracers for imaging phosphodiesterases. *Curr. Top. Med. Chem.* **2012**, *12*, 1224–1236. [[CrossRef](#)] [[PubMed](#)]
26. Martins, T.J.; Mumby, M.C.; Beavo, J.A. Purification and characterization of a cyclic GMP-stimulated cyclic nucleotide phosphodiesterase from bovine tissues. *J. Biol. Chem.* **1982**, *257*, 1973–1979. [[PubMed](#)]
27. Pyne, N.J.; Cooper, M.E.; Houslay, M.D. Identification and characterization of both the cytosolic and particulate forms of cyclic GMP-stimulated cyclic AMP phosphodiesterase from rat liver. *Biochem. J.* **1986**, *234*, 325–334. [[CrossRef](#)] [[PubMed](#)]
28. Russwurm, C.; Zoidl, G.; Koesling, D.; Russwurm, M. Dual acylation of PDE2A splice variant 3: Targeting to synaptic membranes. *J. Biol. Chem.* **2009**, *284*, 25782–25790. [[CrossRef](#)] [[PubMed](#)]
29. Martinez, S.E.; Wu, A.Y.; Glavas, N.A.; Tang, X.B.; Turley, S.; Hol, W.G.; Beavo, J.A. The two GAF domains in phosphodiesterase 2A have distinct roles in dimerization and in cGMP binding. *Proc. Natl. Acad. Sci. USA* **2002**, *99*, 13260–13265. [[CrossRef](#)] [[PubMed](#)]
30. Iffland, A.; Kohls, D.; Low, S.; Luan, J.; Zhang, Y.; Kothe, M.; Cao, Q.; Kamath, A.V.; Ding, Y.-H.; Ellenberger, T. Structural determinants for inhibitor specificity and selectivity in PDE2A using the wheat germ *in vitro* translation system. *Biochemistry* **2005**, *44*, 8312–8325. [[CrossRef](#)] [[PubMed](#)]
31. Pandit, J.; Forman, M.D.; Fennell, K.F.; Dillman, K.S.; Menniti, F.S. Mechanism for the allosteric regulation of phosphodiesterase 2A deduced from the X-ray structure of a near full-length construct. *Proc. Natl. Acad. Sci. USA* **2009**, *106*, 18225–18230. [[CrossRef](#)] [[PubMed](#)]
32. DeNinno, M.P. Future directions in phosphodiesterase drug discovery. *Bioorg. Med. Chem. Lett.* **2012**, *22*, 6794–6800. [[CrossRef](#)] [[PubMed](#)]
33. Kelly, M.P.; Adamowicz, W.; Bove, S.; Hartman, A.J.; Mariga, A.; Pathak, G.; Reinhart, V.; Romegialli, A.; Kleiman, R.J. Select 3',5'-cyclic nucleotide phosphodiesterases exhibit altered expression in the aged rodent brain. *Cell. Signal.* **2014**, *26*, 383–397. [[CrossRef](#)] [[PubMed](#)]
34. Lakics, V.; Karran, E.H.; Boess, F.G. Quantitative comparison of phosphodiesterase mRNA distribution in human brain and peripheral tissues. *Neuropharmacology* **2010**, *59*, 367–374. [[CrossRef](#)] [[PubMed](#)]
35. Menniti, F.S.; Faraci, W.S.; Schmidt, C.J. Phosphodiesterases in the CNS: Targets for drug development. *Nat. Rev. Drug Discov.* **2006**, *5*, 660–670. [[CrossRef](#)] [[PubMed](#)]
36. Sadhu, K.; Hensley, K.; Florio, V.A.; Wolda, S.L. Differential expression of the cyclic GMP-stimulated phosphodiesterase PDE2A in human venous and capillary endothelial cells. *J. Histochem. Cytochem.* **1999**, *47*, 895–906. [[CrossRef](#)] [[PubMed](#)]
37. Morita, H.; Murata, T.; Shimizu, K.; Okumura, K.; Inui, M.; Tagawa, T. Characterization of phosphodiesterase 2A in human malignant melanoma PMP cells. *Oncol. Rep.* **2013**, *29*, 1275–1284. [[CrossRef](#)] [[PubMed](#)]

38. Drees, M.; Zimmermann, R.; Eisenbrand, G. 3',5'-Cyclic nucleotide phosphodiesterase in tumor cells as potential target for tumor growth inhibition. *Cancer Res.* **1993**, *53*, 3058–3061. [[PubMed](#)]
39. Durand, J.; Lampron, A.; Mazzuco, T.L.; Chapman, A.; Bourdeau, I. Characterization of differential gene expression in adrenocortical tumors harboring β -catenin (CTNNB1) mutations. *J. Clin. Endocr. Metab.* **2011**, *96*, E1206–E1211. [[CrossRef](#)] [[PubMed](#)]
40. Dong, H.; Claffey, K.P.; Brocke, S.; Epstein, P.M. Inhibition of breast cancer cell migration by activation of cAMP signaling. *Breast Cancer Res. Treat.* **2015**, *152*, 17–28. [[CrossRef](#)] [[PubMed](#)]
41. Stephenson, D.T.; Coskran, T.M.; Wilhelms, M.B.; Adamowicz, W.O.; O'Donnell, M.M.; Muravnick, K.B.; Menniti, F.S.; Kleiman, R.J.; Morton, D. Immunohistochemical localization of phosphodiesterase 2A in multiple mammalian species. *J. Histochem. Cytochem.* **2009**, *57*, 933–949. [[CrossRef](#)] [[PubMed](#)]
42. Stephenson, D.T.; Coskran, T.M.; Kelly, M.P.; Kleiman, R.J.; Morton, D.; O'Neill, S.M.; Schmidt, C.J.; Weinberg, R.J.; Menniti, F.S. The distribution of phosphodiesterase 2A in the rat brain. *Neuroscience* **2012**, *226*, 145–155. [[CrossRef](#)] [[PubMed](#)]
43. Stange, H.; Langen, B.; Egerland, U.; Hoefgen, N.; Priebs, M.; Malamas, M.S.; Erdel, J.J.; Ni, Y. Triazine Derivatives as Inhibitors of Phosphodiesterases. WO 2010/054253 A1, PCT/US2009/063633, 14 May 2010.
44. Van Staveren, W.C.G.; Markerink-van Ittersum, M.; Steinbusch, H.W.M.; de Vente, J. The effects of phosphodiesterase inhibition on cyclic GMP and cyclic AMP accumulation in the hippocampus of the rat. *Brain Res.* **2001**, *888*, 275–286. [[CrossRef](#)]
45. Suvarna, N.U.; O'Donnell, J.M. Hydrolysis of *N*-methyl-D-aspartate receptor-stimulated cAMP and cGMP by PDE4 and PDE2 phosphodiesterases in primary neuronal cultures of rat cerebral cortex and hippocampus. *J. Pharmacol. Exp. Ther.* **2002**, *302*, 249–256. [[CrossRef](#)] [[PubMed](#)]
46. Blokland, A.; Schreiber, R.; Prickaerts, J. Improving memory: A role for phosphodiesterases. *Curr. Pharm. Des.* **2006**, *12*, 2511–2523. [[CrossRef](#)] [[PubMed](#)]
47. Van Staveren, W.C.G.; Steinbusch, H.W.M.; Markerink-Van Ittersum, M.; Repaske, D.R.; Goy, M.F.; Kotera, J.; Omori, K.; Beavo, J.A.; de Vente, J. mRNA expression patterns of the cGMP-hydrolyzing phosphodiesterases types 2, 5, and 9 during development of the rat brain. *J. Comp. Neurol.* **2003**, *467*, 566–580. [[CrossRef](#)] [[PubMed](#)]
48. Gomez, L.; Breitenbucher, J.G. PDE2 inhibition: Potential for the treatment of cognitive disorders. *Bioorg. Med. Chem. Lett.* **2013**, *23*, 6522–6527. [[CrossRef](#)] [[PubMed](#)]
49. Zhang, C.; Yu, Y.; Ruan, L.; Wang, C.; Pan, J.; Klabnik, J.; Lueptow, L.; Zhang, H.-T.; O'Donnell, J.M.; Xu, Y. The roles of phosphodiesterase 2 in the central nervous and peripheral systems. *Curr. Pharm. Des.* **2015**, *21*, 274–290. [[CrossRef](#)]
50. Masood, A.; Huang, Y.; Hajjhussein, H.; Xiao, L.; Li, H.; Wang, W.; Hamza, A.; Zhan, C.-G.; O'Donnell, J.M. Anxiolytic effects of phosphodiesterase-2 inhibitors associated with increased cGMP signaling. *J. Pharmacol. Exp. Ther.* **2009**, *331*, 690–699. [[CrossRef](#)] [[PubMed](#)]
51. Fernández-Fernández, D.; Rosenbrock, H.; Kroker, K.S. Inhibition of PDE2A, but not PDE9A, modulates presynaptic short-term plasticity measured by paired-pulse facilitation in the CA1 region of the hippocampus. *Synapse* **2015**, *69*, 484–496. [[CrossRef](#)] [[PubMed](#)]
52. Boess, F.G.; Hendrix, M.; van der Staay, F.J.; Erb, C.; Schreiber, R.; van Staveren, W.; de Vente, J.; Prickaerts, J.; Blokland, A.; Koenig, G. Inhibition of phosphodiesterase 2 increases neuronal cGMP, synaptic plasticity and memory performance. *Neuropharmacology* **2004**, *47*, 1081–1092. [[CrossRef](#)] [[PubMed](#)]
53. Reneerkens, O.A.H.; Rutten, K.; Bollen, E.; Hage, T.; Blokland, A.; Steinbusch, H.W.M.; Prickaerts, J. Inhibition of phosphodiesterase type 2 or type 10 reverses object memory deficits induced by scopolamine or MK-801. *Behav. Brain Res.* **2013**, *236*, 16–22. [[CrossRef](#)] [[PubMed](#)]
54. Bales, K.; Plath, N.; Svenstrup, N.; Menniti, F. Phosphodiesterase inhibition to target the synaptic dysfunction in Alzheimer's disease. In *Neurodegenerative Diseases*; Dominguez, C., Ed.; Springer: Berlin/Heidelberg, Germany, 2010; Volume 6, pp. 57–90.
55. Andrés, J.I.; Rombouts, F.J.R.; Trabanco, A.A.; Vanhoof, G.C.P.; De Angelis, M.; Buijsters, P.J.J.A.; Guillemont, J.E.G.; Bormans, G.M.R.; Celen, S.J.L. 1-Aryl-4-methyl-[1,2,4]triazolo[4,3-*a*]quinoxaline derivatives. WO 2013/000924 A1, PCT/EP2012/062381, 3 January 2013.

56. Zhang, L.; Villalobos, A.; Beck, E.M.; Bocan, T.; Chappie, T.A.; Chen, L.; Grimwood, S.; Heck, S.D.; Helal, C.J.; Hou, X.; *et al.* Design and selection parameters to accelerate the discovery of novel central nervous system positron emission tomography (PET) ligands and their application in the development of a novel phosphodiesterase 2A PET ligand. *J. Med. Chem.* **2013**, *56*, 4568–4579. [[CrossRef](#)] [[PubMed](#)]
57. Morley, T.; Massif, C.; Papin, C.; Carroll, V.; Alagille, D.; Baldwin, R.M.; Tamagnan, G. Improved production of [¹⁸F]PF-05270430 for clinical imaging of PDE2A in brain. In Proceedings of the 21st International Symposium on Radiopharmaceutical Sciences, Columbia, MO, USA, 26–31 May 2015; 199, p. S199.
58. Naganawa, M.; Nabulsi, N.; Waterhouse, R.; Lin, S.-F.; Zhang, L.; Cass, T.; Ropchan, J.; McCarthy, T.; Huang, Y.; Carson, R. Human PET studies with [¹⁸F]PF-05270430, a PET radiotracer for imaging phosphodiesterase-2A. *J. Nucl. Med.* **2013**, *54*, 201.
59. Naganawa, M.; Waterhouse, R.N.; Nabulsi, N.B.; Lin, S.-F.; Labaree, D.; Ropchan, J.; Tarabar, S.; DeMartinis, N.; Ogden, A.; Banerjee, A.; *et al.* First in human assessment of the novel PDE2A PET radiotracer ¹⁸F-PF-05270430. *J. Nucl. Med.* **2016**, in press. [[CrossRef](#)] [[PubMed](#)]
60. Schröder, S.; Wenzel, B.; Kranz, M.; Egerland, U.; Teodoro, R.; Deuther-Conrad, W.; Fischer, S.; Höfgen, N.; Steinbach, J.; Brust, P. Development, synthesis and F-18 labelling of a fluoroalkylated triazine derivative for PET imaging of phosphodiesterase 2A. In Proceedings of the Annual Congress of the European Association of Nuclear Medicine, Gothenburg, Sweden, 18–22 October 2014; OP162, p. S197.
61. Schröder, S.; Wenzel, B.; Deuther-Conrad, W.; Teodoro, R.; Egerland, U.; Kranz, M.; Scheunemann, M.; Höfgen, N.; Steinbach, J.; Brust, P. Synthesis, ¹⁸F-radiolabelling and biological characterization of novel fluoroalkylated triazine derivatives for *in vivo* imaging of phosphodiesterase 2A in brain via positron emission tomography. *Molecules* **2015**, *20*, 9591–9615. [[CrossRef](#)] [[PubMed](#)]
62. Schröder, S.; Wenzel, B.; Deuther-Conrad, W.; Teodoro, R.; Egerland, U.; Kranz, M.; Fischer, S.; Höfgen, N.; Steinbach, J.; Brust, P. Novel ¹⁸F-labelled triazine derivatives for PET imaging of phosphodiesterase 2A. In Proceedings of the 21st International Symposium on Radiopharmaceutical Sciences, Columbia, MO, USA, 26–31 May 2015; 221, p. S221.
63. Zoghbi, S.S.; Shetty, H.U.; Ichise, M.; Fujita, M.; Imaizumi, M.; Liow, J.-S.; Shah, J.; Musachio, J.L.; Pike, V.W.; Innis, R.B. PET imaging of the dopamine transporter with [¹⁸F]FECNT: A polar radiometabolite confounds brain radioligand measurements. *J. Nucl. Med.* **2006**, *47*, 520–527. [[PubMed](#)]
64. Evens, N.; Vandeputte, C.; Muccioli, G.G.; Lambert, D.M.; Baekelandt, V.; Verbruggen, A.M.; Debyser, Z.; van Laere, K.; Bormans, G.M. Synthesis, *in vitro* and *in vivo* evaluation of fluorine-18 labelled FE-GW405833 as a PET tracer for type 2 cannabinoid receptor imaging. *Bioorg. Med. Chem.* **2011**, *19*, 4499–4505. [[CrossRef](#)] [[PubMed](#)]
65. Bolger, G.B.; Rodgers, L.; Riggs, M. Differential CNS expression of alternative mRNA isoforms of the mammalian genes encoding cAMP-specific phosphodiesterases. *Gene* **1994**, *149*, 237–244. [[CrossRef](#)]
66. Horton, Y.M.; Sullivan, M.; Houslay, M.D. Molecular cloning of a novel splice variant of human type IVA (PDE-IVA) cyclic AMP phosphodiesterase and localization of the gene to the p13.2-q12 region of human chromosome 19. *Biochem. J.* **1995**, *308*, 683–691. [[CrossRef](#)] [[PubMed](#)]
67. Kenk, M.; Thomas, A.; Lortie, M.; deKemp, R.; Beanlands, R.S.; DaSilva, J.N. PET measurements of cAMP-mediated phosphodiesterase-4 with (R)-[¹¹C]rolipram. *Curr. Radiopharm.* **2011**, *4*, 44–58. [[CrossRef](#)] [[PubMed](#)]
68. Pérez-Torres, S.; Miró, X.; Palacios, J.M.; Cortés, R.; Puigdoménech, P.; Mengod, G. Phosphodiesterase type 4 isozymes expression in human brain examined by *in situ* hybridization histochemistry and [³H]rolipram binding autoradiography: Comparison with monkey and rat brain. *J. Chem. Neuroanat.* **2000**, *20*, 349–374. [[CrossRef](#)]
69. Bureau, Y.; Handa, M.; Zhu, Y.; Laliberte, F.; Moore, C.S.; Liu, S.; Huang, Z.; MacDonald, D.; Xu, D.G.; Robertson, G.S. Neuroanatomical and pharmacological assessment of Fos expression induced in the rat brain by the phosphodiesterase-4 inhibitor 6-(4-pyridylmethyl)-8-(3-nitrophenyl)quinoline. *Neuropharmacology* **2006**, *51*, 974–985. [[CrossRef](#)] [[PubMed](#)]
70. Souness, J.E.; Griffin, M.; Maslen, C.; Ebsworth, K.; Scott, L.C.; Pollock, K.; Palfreyman, M.N.; Karlsson, J.A. Evidence that cyclic AMP phosphodiesterase inhibitors suppress TNF alpha generation from human monocytes by interacting with a ‘low-affinity’ phosphodiesterase 4 conformer. *Br. J. Pharmacol.* **1996**, *118*, 649–658. [[CrossRef](#)]

71. Reyes-Irisarri, E.; Sanchez, A.J.; Garcia-Merino, J.A.; Mengod, G. Selective induction of cAMP phosphodiesterase PDE4B2 expression in experimental autoimmune encephalomyelitis. *J. Neuropath. Exp. Neur.* **2007**, *66*, 923–931. [[CrossRef](#)] [[PubMed](#)]
72. Barnette, M.S.; Bartus, J.O.; Burman, M.; Christensen, S.B.; Cieslinski, L.B.; Esser, K.M.; Prabhakar, U.S.; Rush, J.A.; Torphy, T.J. Association of the anti-inflammatory activity of phosphodiesterase 4 (PDE4) inhibitors with either inhibition of PDE4 catalytic activity or competition for [³H]rolipram binding. *Biochem. Pharmacol.* **1996**, *51*, 949–956. [[PubMed](#)]
73. Johnson-Mills, K.; Arauz, E.; Coffey, R.G.; Krzanowski, J.J., Jr.; Polson, J.B. Effect of CI-930 (3-(2H)-pyridazinone-4,5-dihydro-6-(4-(1H-imidazolyl)phenyl)-5-methyl-mono-hydrochloride) and rolipram on human coronary artery smooth muscle cell proliferation. *Biochem. Pharmacol.* **1998**, *56*, 1065–1073. [[CrossRef](#)]
74. Gurney, M.E.; D’Amato, E.C.; Burgin, A.B. Phosphodiesterase-4 (PDE4) molecular pharmacology and Alzheimer’s disease. *Neurotherapeutics* **2015**, *12*, 49–56. [[CrossRef](#)] [[PubMed](#)]
75. Dyke, H.J.; Montana, J.G. Update on the therapeutic potential of PDE4 inhibitors. *Expert Opin. Investig. Drugs* **2002**, *11*, 1–13. [[PubMed](#)]
76. Saldou, N.; Obernolte, R.; Huber, A.; Baecker, P.A.; Wilhelm, R.; Alvarez, R.; Li, B.; Xia, L.; Callan, O.; Su, C.; *et al.* Comparison of recombinant human PDE4 isoforms: Interaction with substrate and inhibitors. *Cell. Signal.* **1998**, *10*, 427–440. [[CrossRef](#)]
77. Wang, P.; Myers, J.G.; Wu, P.; Cheewatrakoolpong, B.; Egan, R.W.; Billah, M.M. Expression, purification, and characterization of human cAMP-specific phosphodiesterase (PDE4) subtypes A, B, C, and D. *Biochem. Bioph. Res. Commun.* **1997**, *234*, 320–324. [[CrossRef](#)] [[PubMed](#)]
78. Gale, D.D.; Hofer, P.; Spina, D.; Seeds, E.A.; Banner, K.H.; Harrison, S.; Douglas, G.; Matsumoto, T.; Page, C.P.; Wong, R.H.; *et al.* Pharmacology of a new cyclic nucleotide phosphodiesterase type 4 inhibitor, V11294. *Pulm. Pharmacol. Ther.* **2003**, *16*, 97–104. [[CrossRef](#)]
79. DaSilva, J.N.; Lourenco, C.M.; Wilson, A.A.; Houle, S. Syntheses of the phosphodiesterase-4 inhibitors [¹¹C]Ro 20–1724, R-, R/S- and S-[¹¹C]rolipram. *J. Label. Comp. Radiopharm.* **2001**, *44*, 373–384. [[CrossRef](#)]
80. Fujita, M.; Hines, C.S.; Zoghbi, S.S.; Mallinger, A.G.; Dickstein, L.P.; Liow, J.S.; Zhang, Y.; Pike, V.W.; Drevets, W.C.; Innis, R.B.; *et al.* Downregulation of brain phosphodiesterase type IV measured with ¹¹C-(R)-rolipram positron emission tomography in major depressive disorder. *Biol. Psychiat.* **2012**, *72*, 548–554. [[CrossRef](#)] [[PubMed](#)]
81. Lortie, M.; DaSilva, J.N.; Kenk, M.; Thorn, S.; Davis, D.; Birnie, D.; Beanlands, R.S.; deKemp, R.A. Analysis of (R)- and (S)-[¹¹C]rolipram kinetics in canine myocardium for the evaluation of phosphodiesterase-4 with PET. *Mol. Imaging Biol.* **2012**, *14*, 225–236. [[CrossRef](#)] [[PubMed](#)]
82. Thomae, D.; Papin, C.; Morley, T.; Alagille, D.; Barret, O.; Lee, H.; Baldwin, R.M.; Tamagnan, G. Identification and *in vivo* evaluation of [¹⁸F]MNI-617 as a radioligand for PDE4 imaging in non human primate. In Proceedings of the 21st International Symposium on Radiopharmaceutical Sciences, Columbia, MO, USA, 26–31 May 2015; 235, p. S235.
83. Thomae, D.; Morley, T.J.; Lee, H.S.; Barret, O.; Constantinescu, C.; Papin, C.; Baldwin, R.M.; Tamagnan, G.D.; Alagille, D. Identification and *in vivo* evaluation of a fluorine-18 rolipram analogue, [¹⁸F]MNI-617, as a radioligand for PDE4 imaging in mammalian brain. *J. Label. Comp. Radiopharm.* **2016**. [[CrossRef](#)] [[PubMed](#)]
84. Kuchar, M.; Mamat, C. Methods to increase the metabolic stability of ¹⁸F-radiotracers. *Molecules* **2015**, *20*, 16186. [[CrossRef](#)] [[PubMed](#)]
85. Sopory, S.; Kaur, T.; Visweswariah, S.S. The cGMP-binding, cGMP-specific phosphodiesterase (PDE5): Intestinal cell expression, regulation and role in fluid secretion. *Cell. Signal.* **2004**, *16*, 681–692. [[CrossRef](#)] [[PubMed](#)]
86. Turko, I.V.; Haik, T.L.; McAllister-Lucas, L.M.; Burns, F.; Francis, S.H.; Corbin, J.D. Identification of key amino acids in a conserved cGMP-binding site of cGMP-binding phosphodiesterases. A putative NKXnD motif for cGMP binding. *J. Biol. Chem.* **1996**, *271*, 22240–22244. [[PubMed](#)]
87. Lin, C.S.; Lin, G.; Xin, Z.C.; Lue, T.F. Expression, distribution and regulation of phosphodiesterase 5. *Curr. Pharm. Des.* **2006**, *12*, 3439–3457. [[CrossRef](#)]
88. Giovannoni, M.P.; Vergelli, C.; Graziano, A.; Dal Piaz, V. PDE5 inhibitors and their applications. *Curr. Med. Chem.* **2010**, *17*, 2564–2587. [[CrossRef](#)] [[PubMed](#)]

89. Buckley, M.S.; Staib, R.L.; Wicks, L.M.; Feldman, J.P. Phosphodiesterase-5 inhibitors in management of pulmonary hypertension: Safety, tolerability, and efficacy. *Drug Healthc. Patient Saf.* **2010**, *2*, 151–161. [[PubMed](#)]
90. Evans, J.D.; Hill, S.R. A comparison of the available phosphodiesterase-5 inhibitors in the treatment of erectile dysfunction: A focus on avanafil. *Patient Prefer. Adher.* **2015**, *9*, 1159–1164. [[CrossRef](#)] [[PubMed](#)]
91. Pokreisz, P.; Vandenwijngaert, S.; Bito, V.; Van den Bergh, A.; Lenaerts, I.; Busch, C.; Marsboom, G.; Gheysens, O.; Vermeersch, P.; Biesmans, L.; *et al.* Ventricular phosphodiesterase-5 expression is increased in patients with advanced heart failure and contributes to adverse ventricular remodeling after myocardial infarction in mice. *Circulation* **2009**, *119*, 408–416. [[CrossRef](#)] [[PubMed](#)]
92. Takimoto, E.; Champion, H.C.; Li, M.; Belardi, D.; Ren, S.; Rodriguez, E.R.; Bedja, D.; Gabrielson, K.L.; Wang, Y.; Kass, D.A. Chronic inhibition of cyclic GMP phosphodiesterase 5A prevents and reverses cardiac hypertrophy. *Nat. Med.* **2005**, *11*, 214–222. [[CrossRef](#)] [[PubMed](#)]
93. Salloum, F.N.; Ockaili, R.A.; Wittkamp, M.; Marwaha, V.R.; Kukreja, R.C. Vardenafil: A novel type 5 phosphodiesterase inhibitor reduces myocardial infarct size following ischemia/reperfusion injury via opening of mitochondrial KATP channels in rabbits. *J. Mol. Cell. Cardiol.* **2006**, *40*, 405–411. [[CrossRef](#)] [[PubMed](#)]
94. Das, A.; Durrant, D.; Salloum, F.N.; Xi, L.; Kukreja, R.C. PDE5 inhibitors as therapeutics for heart disease, diabetes and cancer. *Pharmacol. Ther.* **2015**, *147*, 12–21. [[CrossRef](#)] [[PubMed](#)]
95. Chekol, R.; Gheysens, O.; Cleyhens, J.; Janssens, S.; Verbruggen, A.; Bormans, G. Radiosynthesis and biological evaluation of a carbon-11 labelled vardenafil derivative as a PDE5 specific tracer. In Proceedings of the 19th International Symposium on Radiopharmaceutical Sciences, Amsterdam, The Netherlands, 28 August–2 September 2011; P-063, p. S152.
96. Chekol, R.; Gheysens, O.; Cleyhens, J.; Janssens, S.; Verbruggen, A.; Bormans, G. Labelling and preliminary biological evaluation of [¹¹C]RBQ08 as a specific PDE5 radiotracer. In Proceedings of the 19th International Symposium on Radiopharmaceutical Sciences, Amsterdam, the Netherlands, 28 August–2 September 2011; P-064, p. S153.
97. Chekol, R.; Gheysens, O.; Cleyhens, J.; Pokreisz, P.; Vanhoof, G.; Ahamed, M.; Janssens, S.; Verbruggen, A.; Bormans, G. Evaluation of PET radioligands for *in vivo* visualization of phosphodiesterase 5 (PDE5). *Nucl. Med. Biol.* **2014**, *41*, 155–162. [[CrossRef](#)] [[PubMed](#)]
98. Bi, Y.; Stoy, P.; Adam, L.; He, B.; Krupinski, J.; Normandin, D.; Pongrac, R.; Seliger, L.; Watson, A.; Macor, J.E. Quinolines as extremely potent and selective PDE5 inhibitors as potential agents for treatment of erectile dysfunction. *Bioorg. Med. Chem. Lett.* **2004**, *14*, 1577–1580. [[CrossRef](#)] [[PubMed](#)]
99. Tollefson, M.B.; Acker, B.A.; Jacobsen, E.J.; Hughes, R.O.; Walker, J.K.; Fox, D.N.A.; Palmer, M.J.; Freeman, S.K.; Yu, Y.; Bond, B.R. 1-(2-Ethoxyethyl)-1H-pyrazolo[4,3-d]pyrimidines as potent phosphodiesterase 5 (PDE5) inhibitors. *Bioorg. Med. Chem. Lett.* **2010**, *20*, 3120–3124. [[CrossRef](#)] [[PubMed](#)]
100. Kotera, J.; Fujishige, K.; Omori, K. Immunohistochemical localization of cGMP-binding cGMP-specific phosphodiesterase (PDE5) in rat tissues. *J. Histochem. Cytochem.* **2000**, *48*, 685–693. [[CrossRef](#)] [[PubMed](#)]
101. Bender, A.T.; Beavo, J.A. Specific localized expression of cGMP PDEs in Purkinje neurons and macrophages. *Neurochem. Int.* **2004**, *45*, 853–857. [[CrossRef](#)] [[PubMed](#)]
102. Peixoto, C.A.; Nunes, A.K.S.; Garcia-Osta, A. Phosphodiesterase-5 inhibitors: Action on the signaling pathways of neuroinflammation, neurodegeneration, and cognition. *Mediat. Inflamm.* **2015**, *2015*, 940207. [[CrossRef](#)] [[PubMed](#)]
103. Puerta, E.; Hervias, I.; Goni-Allo, B.; Lasheras, B.; Jordan, J.; Aguirre, N. Phosphodiesterase 5 inhibitors prevent 3,4-methylenedioxymethamphetamine-induced 5-HT deficits in the rat. *J. Neurochem.* **2009**, *108*, 755–766. [[CrossRef](#)] [[PubMed](#)]
104. Puerta, E.; Hervias, I.; Barros-Minones, L.; Jordan, J.; Ricobaraza, A.; Cuadrado-Tejedor, M.; Garcia-Osta, A.; Aguirre, N. Sildenafil protects against 3-nitropropionic acid neurotoxicity through the modulation of calpain, CREB, and BDNF. *Neurobiol. Dis.* **2010**, *38*, 237–245. [[CrossRef](#)] [[PubMed](#)]
105. Puerta, E.; Barros-Minones, L.; Hervias, I.; Gomez-Rodriguez, V.; Orejana, L.; Pizarro, N.; de la Torre, R.; Jordan, J.; Aguirre, N. Long-lasting neuroprotective effect of sildenafil against 3,4-methylenedioxymethamphetamine-induced 5-hydroxytryptamine deficits in the rat brain. *J. Neurosci. Res.* **2012**, *90*, 518–528. [[CrossRef](#)] [[PubMed](#)]

106. Barros-Minones, L.; Orejana, L.; Goni-Allo, B.; Suquia, V.; Hervias, I.; Aguirre, N.; Puerta, E. Modulation of the ASK1-MKK3/6-p38/MAPK signalling pathway mediates sildenafil protection against chemical hypoxia caused by malonate. *Br. J. Pharmacol.* **2013**, *168*, 1820–1834. [[CrossRef](#)] [[PubMed](#)]
107. Puzzo, D.; Staniszewski, A.; Deng, S.X.; Privitera, L.; Leznik, E.; Liu, S.; Zhang, H.; Feng, Y.; Palmeri, A.; Landry, D.W.; *et al.* Phosphodiesterase 5 inhibition improves synaptic function, memory, and amyloid-beta load in an Alzheimer's disease mouse model. *J. Neurosci.* **2009**, *29*, 8075–8086. [[CrossRef](#)] [[PubMed](#)]
108. Cuadrado-Tejedor, M.; Hervias, I.; Ricobaraza, A.; Puerta, E.; Perez-Roldan, J.M.; Garcia-Barroso, C.; Franco, R.; Aguirre, N.; Garcia-Osta, A. Sildenafil restores cognitive function without affecting β -amyloid burden in a mouse model of Alzheimer's disease. *Br. J. Pharmacol.* **2011**, *164*, 2029–2041. [[CrossRef](#)] [[PubMed](#)]
109. Gómez-Vallejo, V.; Ugarte, A.; García-Barroso, C.; Cuadrado-Tejedor, M.; Szczupak, B.; Dopeso-Reyes, I.G.; Lanciego, J.L.; García-Osta, A.; Llop, J.; Oyarzabal, J.; *et al.* Pharmacokinetic investigation of sildenafil using positron emission tomography and determination of its effect on cerebrospinal fluid cGMP levels. *J. Neurochem.* **2016**, *136*, 403–415. [[CrossRef](#)] [[PubMed](#)]
110. Liu, J.; Wenzel, B.; Dukic-Stefanovic, S.; Teodoro, R.; Ludwig, F.-A.; Deuther-Conrad, W.; Schröder, S.; Chezal, J.-M.; Moreau, E.; Brust, P.; *et al.* Development of a new radiofluorinated quinoline analog for PET imaging of phosphodiesterase 5 (PDE5) in brain. *Pharmaceuticals* **2016**, *9*, 22. [[CrossRef](#)] [[PubMed](#)]
111. Loughney, K.; Hill, T.R.; Florio, V.A.; Uher, L.; Rosman, G.J.; Wolda, S.L.; A. Jones, B.; Howard, M.L.; McAllister-Lucas, L.M.; Sonnenburg, W.K.; *et al.* Isolation and characterization of cDNAs encoding PDE5A, a human cGMP-binding, cGMP-specific 3',5'-cyclic nucleotide phosphodiesterase. *Gene* **1998**, *216*, 139–147. [[CrossRef](#)]
112. Cumming, P. A business of some heat: Molecular imaging of phosphodiesterase 5. *J. Neurochem.* **2016**, *136*, 220–221. [[CrossRef](#)] [[PubMed](#)]
113. Miro, X.; Perez-Torres, S.; Palacios, J.M.; Puigdomenech, P.; Mengod, G. Differential distribution of cAMP-specific phosphodiesterase 7A mRNA in rat brain and peripheral organs. *Synapse* **2001**, *40*, 201–214. [[CrossRef](#)] [[PubMed](#)]
114. Johansson, E.M.; Reyes-Irisarri, E.; Mengod, G. Comparison of cAMP-specific phosphodiesterase mRNAs distribution in mouse and rat brain. *Neurosci. Lett.* **2012**, *525*, 1–6. [[CrossRef](#)] [[PubMed](#)]
115. Reyes-Irisarri, E.; Perez-Torres, S.; Mengod, G. Neuronal expression of cAMP-specific phosphodiesterase 7B mRNA in the rat brain. *Neuroscience* **2005**, *132*, 1173–1185. [[CrossRef](#)] [[PubMed](#)]
116. Nakata, A.; Ogawa, K.; Sasaki, T.; Koyama, N.; Wada, K.; Kotera, J.; Kikkawa, H.; Omori, K.; Kaminuma, O. Potential role of phosphodiesterase 7 in human T cell function: Comparative effects of two phosphodiesterase inhibitors. *Clin. Exp. Immunol.* **2002**, *128*, 460–466. [[CrossRef](#)] [[PubMed](#)]
117. Morales-Garcia, J.A.; Redondo, M.; Alonso-Gil, S.; Gil, C.; Perez, C.; Martinez, A.; Santos, A.; Perez-Castillo, A. Phosphodiesterase 7 inhibition preserves dopaminergic neurons in cellular and rodent models of Parkinson disease. *PLoS ONE* **2011**, *6*, e17240. [[CrossRef](#)] [[PubMed](#)]
118. Demopulos, G.A.; Gaitanaris, G.A. Treatment of Addiction and Impulse-Control Disorders Using PDE7 Inhibitors. WO2012/064667 A3, 14 November 2013.
119. Gil, C.; Campillo, N.E.; Perez, D.I.; Martinez, A. PDE7 inhibitors as new drugs for neurological and inflammatory disorders. *Expert Opin. Ther. Pat.* **2008**, *18*, 1127–1139. [[CrossRef](#)]
120. De Gortari, P.; Mengod, G. Dopamine D1, D2 and mu-opioid receptors are co-expressed with adenylyl cyclase 5 and phosphodiesterase 7B mRNAs in striatal rat cells. *Brain Res.* **2010**, *1310*, 37–45. [[CrossRef](#)] [[PubMed](#)]
121. Thomae, D.; Servaes, S.; Vazquez, N.; Wyffels, L.; Dedeurwaerdere, S.; van der Veken, P.; Joossens, J.; Augustyns, K.; Stroobants, S.; Staelens, S. Synthesis and preclinical evaluation of two novel radioligands for PDE7 imaging in the brain. In Proceedings of the 21st International Symposium on Radiopharmaceutical Sciences, Columbia, MO, USA, 26–31 May 2015; 295, p. S295.
122. Thomae, D.; Servaes, S.; Vazquez, N.; Wyffels, L.; Dedeurwaerdere, S.; Van der Veken, P.; Joossens, J.; Augustyns, K.; Stroobants, S.; Staelens, S. Synthesis and preclinical evaluation of an ^{18}F labeled PDE7 inhibitor for PET neuroimaging. *Nucl. Med. Biol.* **2015**, *42*, 975–981. [[CrossRef](#)] [[PubMed](#)]
123. Bernardelli, P.; Lorthiois, E.; Vergne, F.; Oliveira, C.; Mafroud, A.K.; Proust, E.; Pham, N.; Ducrot, P.; Moreau, F.; Idrissi, M.; *et al.* Spiroquinazolinones as novel, potent, and selective PDE7 inhibitors. Part 2: Optimization of 5,8-disubstituted derivatives. *Bioorg. Med. Chem. Lett.* **2004**, *14*, 4627–4631. [[CrossRef](#)] [[PubMed](#)]

124. Fujishige, K.; Kotera, J.; Omori, K. Striatum- and testis-specific phosphodiesterase PDE10A. *Eur. J. Biochem.* **1999**, *266*, 1118–1127. [[CrossRef](#)] [[PubMed](#)]
125. Fujishige, K.; Kotera, J.; Michibata, H.; Yuasa, K.; Takebayashi, S.-I.; Okumura, K.; Omori, K. Cloning and characterization of a novel human phosphodiesterase that hydrolyzes both cAMP and cGMP (PDE10A). *J. Biol. Chem.* **1999**, *274*, 18438–18445. [[CrossRef](#)] [[PubMed](#)]
126. Kotera, J.; Fujishige, K.; Yuasa, K.; Omori, K. Characterization and phosphorylation of PDE10A2, a novel alternative splice variant of human phosphodiesterase that hydrolyzes cAMP and cGMP. *Biochem. Biophys. Res. Commun.* **1999**, *261*, 551–557. [[CrossRef](#)] [[PubMed](#)]
127. Kotera, J.; Sasaki, T.; Kobayashi, T.; Fujishige, K.; Yamashita, Y.; Omori, K. Subcellular localization of cyclic nucleotide phosphodiesterase type 10A variants, and alteration of the localization by cAMP-dependent protein kinase-dependent phosphorylation. *J. Biol. Chem.* **2004**, *279*, 4366–4375. [[CrossRef](#)] [[PubMed](#)]
128. Jäger, R.; Russwurm, C.; Schwede, F.; Genieser, H.-G.; Koesling, D.; Russwurm, M. Activation of PDE10 and PDE11 phosphodiesterases. *J. Biol. Chem.* **2012**, *287*, 1210–1219. [[CrossRef](#)] [[PubMed](#)]
129. Gross-Langenhoff, M.; Hofbauer, K.; Weber, J.; Schultz, A.; Schultz, J.E. CAMP is a ligand for the tandem GAF domain of human phosphodiesterase 10 and cGMP for the tandem GAF domain of phosphodiesterase 11. *J. Biol. Chem.* **2006**, *281*, 2841–2846. [[CrossRef](#)] [[PubMed](#)]
130. Seeger, T.F.; Bartlett, B.; Coskran, T.M.; Culp, J.S.; James, L.C.; Krull, D.L.; Lanfear, J.; Ryan, A.M.; Schmidt, C.J.; Strick, C.A.; *et al.* Immunohistochemical localization of PDE10A in the rat brain. *Brain Res.* **2003**, *985*, 113–126. [[CrossRef](#)]
131. Coskran, T.M.; Morton, D.; Menniti, F.S.; Adamowicz, W.O.; Kleiman, R.J.; Ryan, A.M.; Strick, C.A.; Schmidt, C.J.; Stephenson, D.T. Immunohistochemical localization of phosphodiesterase 10A in multiple mammalian species. *J. Histochem. Cytochem.* **2006**, *54*, 1205–1213. [[CrossRef](#)] [[PubMed](#)]
132. Bollen, E.; Prickaerts, J. Phosphodiesterases in neurodegenerative disorders. *IUBMB Life* **2012**, *64*, 965–970. [[CrossRef](#)] [[PubMed](#)]
133. Kehler, J.; Nielsen, J. PDE10A inhibitors: Novel therapeutic drugs for schizophrenia. *Curr. Pharm. Des.* **2011**, *17*, 137–150. [[CrossRef](#)]
134. Chappie, T.A.; Helal, C.J.; Hou, X. Current landscape of phosphodiesterase 10A (PDE10A) inhibition. *J. Med. Chem.* **2012**, *55*, 7299–7331. [[CrossRef](#)] [[PubMed](#)]
135. Dedeurwaerdere, S.; Wintmolders, C.; Vanhoof, G.; Langlois, X. Patterns of brain glucose metabolism induced by phosphodiesterase 10A inhibitors in the mouse: A potential translational biomarker. *J. Pharmacol. Exp. Ther.* **2011**, *339*, 210–217. [[CrossRef](#)] [[PubMed](#)]
136. Hoefgen, N.; Grunwald, C.; Langen, B. Targeting PDE10A in schizophrenia. *Drug Future* **2012**, *37*, 577–589. [[CrossRef](#)]
137. Kehler, J.; Kilburn, J.P. Patented PDE10A inhibitors: Novel compounds since 2007. *Expert Opin. Ther. Pat.* **2009**, *19*, 1715–1725. [[CrossRef](#)] [[PubMed](#)]
138. Kehler, J. Phosphodiesterase 10A inhibitors: A 2009–2012 patent update. *Expert Opin. Ther. Pat.* **2013**, *23*, 31–45. [[CrossRef](#)] [[PubMed](#)]
139. Grauer, S.M.; Pulito, V.L.; Navarra, R.L.; Kelly, M.P.; Kelley, C.; Graf, R.; Langen, B.; Logue, S.; Brennan, J.; Jiang, L.; *et al.* Phosphodiesterase 10A inhibitor activity in preclinical models of the positive, cognitive, and negative symptoms of schizophrenia. *J. Pharmacol. Exp. Ther.* **2009**, *331*, 574–590. [[CrossRef](#)] [[PubMed](#)]
140. Verhoest, P.R.; Chapin, D.S.; Corman, M.; Fonseca, K.; Harms, J.F.; Hou, X.; Marr, E.S.; Menniti, F.S.; Nelson, F.; O'Connor, R.; *et al.* Discovery of a novel class of phosphodiesterase 10A inhibitors and identification of clinical candidate 2-(4-(1-methyl-4-pyridin-4-yl-1H-pyrazol-3-yl)-phenoxy)methyl)-quinoline (PF-2545920) for the treatment of schizophrenia. *J. Med. Chem.* **2009**, *52*, 5188–5196. [[CrossRef](#)] [[PubMed](#)]
141. Tu, Z.; Fan, J.; Li, S.; Jones, L.A.; Cui, J.; Padakanti, P.K.; Xu, J.; Zeng, D.; Shoghi, K.I.; Perlmutter, J.S.; *et al.* Radiosynthesis and *in vivo* evaluation of [¹¹C]MP-10 as a PET probe for imaging PDE10A in rodent and non-human primate brain. *Bioorg. Med. Chem.* **2011**, *19*, 1666–1673. [[CrossRef](#)] [[PubMed](#)]
142. Plisson, C.; Weinzimmer, D.; Jakobsen, S.; Natesan, S.; Salinas, C.; Lin, S.F.; Labaree, D.; Zheng, M.Q.; Nabulsi, N.; Marques, T.R.; *et al.* Phosphodiesterase 10A PET radioligand development program: From pig to human. *J. Nucl. Med.* **2014**, *55*, 595–601. [[CrossRef](#)] [[PubMed](#)]
143. Ooms, M.; Celen, S.; Koole, M.; Langlois, X.; Schmidt, M.; de Angelis, M.; Andrés, J.I.; Verbruggen, A.; van Laere, K.; Bormans, G. Synthesis and biological evaluation of carbon-11 and fluorine-18 labeled tracers for *in vivo* visualization of PDE10A. *Nucl. Med. Biol.* **2014**, *41*, 695–704. [[CrossRef](#)] [[PubMed](#)]

144. Ooms, M.; Celen, S.; Verbruggen, A.; van Laere, K.; Bormans, G. Synthesis and preliminary biological evaluation of [¹¹C]-MP10 and its regio-isomer as potential radioligands for positron emission tomography imaging of phosphodiesterase-10A in the brain. *Eur. J. Nucl. Med. Mol. Imaging* **2010**, *37*, S206.
145. Plisson, C.; Salinas, C.; Weinzimmer, D.; Labaree, D.; Lin, S.-F.; Ding, Y.-S.; Jakobsen, S.; Smith, P.W.; Eiji, K.; Carson, R.E.; *et al.* Radiosynthesis and *in vivo* evaluation of [¹¹C]MP-10 as a positron emission tomography radioligand for phosphodiesterase 10A. *Nucl. Med. Biol.* **2011**, *38*, 875–884. [[CrossRef](#)] [[PubMed](#)]
146. Natesan, S.; Ashworth, S.; Nielsen, J.; Tang, S.P.; Salinas, C.; Kealey, S.; Lauridsen, J.B.; Stensbol, T.B.; Gunn, R.N.; Rabiner, E.A.; *et al.* Effect of chronic antipsychotic treatment on striatal phosphodiesterase 10A levels: A [¹¹C]MP-10 PET rodent imaging study with *ex vivo* confirmation. *Transl. Psychiatry* **2014**, *4*, e376. [[CrossRef](#)] [[PubMed](#)]
147. Lin, S.-F.; Labaree, D.; Chen, M.-K.; Holden, D.; Gallezot, J.-D.; Kapinos, M.; Teng, J.-K.; Najafzadeh, S.; Plisson, C.; Rabiner, E.A.; *et al.* Further evaluation of [¹¹C]MP-10 as a radiotracer for phosphodiesterase 10A: PET imaging study in rhesus monkeys and brain tissue metabolite analysis. *Synapse* **2015**, *69*, 86–95. [[CrossRef](#)] [[PubMed](#)]
148. Andrés-Gil, J.I.; Bormans, G.; De Angelis, M.; Celen, S. Radiolabelled PDE10 Ligands. WO 2010/097367 A1, 2 September 2010.
149. Celen, S.; Koole, M.; De Angelis, M.; Sannen, I.; Chitneni, S.K.; Alcazar, J.; Dedeurwaerdere, S.; Moechars, D.; Schmidt, M.; Verbruggen, A.; *et al.* Preclinical evaluation of [¹⁸F]-JNJ41510417 as a radioligand for PET imaging of phosphodiesterase-10A in the brain. *J. Nucl. Med.* **2010**, *51*, 1584–1591. [[CrossRef](#)] [[PubMed](#)]
150. Andrés, J.I.; de Angelis, M.; Alcázar, J.; Iturrino, L.; Langlois, X.; Dedeurwaerdere, S.; Lenaerts, I.; Vanhoof, G.; Celen, S.; Bormans, G. Synthesis, *in vivo* occupancy, and radiolabeling of potent phosphodiesterase subtype-10 inhibitors as candidates for positron emission tomography imaging. *J. Med. Chem.* **2011**, *54*, 5820–5835. [[CrossRef](#)] [[PubMed](#)]
151. Celen, S.; Koole, M.; Ooms, M.; De Angelis, M.; Sannen, I.; Cornelis, J.; Alcazar, J.; Schmidt, M.; Verbruggen, A.; Langlois, X.; *et al.* Preclinical evaluation of [¹⁸F]JNJ42259152 as a PET tracer for PDE10A. *Neuroimage* **2013**, *82*, 13–22. [[CrossRef](#)] [[PubMed](#)]
152. Van Laere, K.; Ahmad, R.U.; Hudyana, H.; Celen, S.; Dubois, K.; Schmidt, M.E.; Bormans, G.; Koole, M. Human biodistribution and dosimetry of [¹⁸F]JNJ42259152, a radioligand for phosphodiesterase 10A imaging. *Eur. J. Nucl. Med. Mol. Imaging* **2012**, *40*, 254–261. [[CrossRef](#)] [[PubMed](#)]
153. Van Laere, K.; Ahmad, R.U.; Hudyana, H.; Dubois, K.; Schmidt, M.E.; Celen, S.; Bormans, G.; Koole, M. Quantification of [¹⁸F]JNJ42259152, a novel phosphodiesterase 10A PET tracer: Kinetic modeling and test–retest study in human brain. *J. Nucl. Med.* **2013**, *54*, 1285–1293. [[CrossRef](#)] [[PubMed](#)]
154. Ahmad, R.; Bourgeois, S.; Postnov, A.; Schmidt, M.E.; Bormans, G.; Van Laere, K.; Vandenberghe, W. PET imaging shows loss of striatal PDE10A in patients with Huntington disease. *Neurology* **2014**, *82*, 279–281. [[CrossRef](#)] [[PubMed](#)]
155. Ooms, M.; Rietjens, R.; Rangarajan, J.R.; Vunckx, K.; Valdeolivas, S.; Maes, F.; Himmelreich, U.; Fernandez-Ruiz, J.; Bormans, G.; Van Laere, K.; *et al.* Early decrease of type 1 cannabinoid receptor binding and phosphodiesterase 10A activity *in vivo* in R6/2 Huntington mice. *Neurobiol. Aging* **2014**, *35*, 2858–2869. [[CrossRef](#)] [[PubMed](#)]
156. Ooms, M.; Celen, S.; De Hoogt, R.; Lenaerts, I.; Liebrechts, J.; Vanhoof, G.; Langlois, X.; Postnov, A.; Koole, M.; Verbruggen, A.; *et al.* Striatal phosphodiesterase 10A availability is altered secondary to chronic changes in dopamine neurotransmission. *EJNMMI Radiopharm. Chem.* **2016**, *1*, 1–17. [[CrossRef](#)]
157. Fan, J.; Zhang, X.; Li, J.; Jin, H.; Padakanti, P.K.; Jones, L.A.; Flores, H.P.; Su, Y.; Perlmutter, J.S.; Tu, Z. Radiosyntheses and *in vivo* evaluation of carbon-11 PET tracers for PDE10A in the brain of rodent and nonhuman primate. *Bioorg. Med. Chem.* **2014**, *22*, 2648–2654. [[CrossRef](#)] [[PubMed](#)]
158. Li, J.; Zhang, X.; Jin, H.; Fan, J.; Flores, H.; Perlmutter, J.S.; Tu, Z. Synthesis of fluorine-containing phosphodiesterase 10A (PDE10A) inhibitors and the *in vivo* evaluation of F-18 labeled PDE10A PET tracers in rodent and nonhuman primate. *J. Med. Chem.* **2015**, *58*, 8584–8600. [[CrossRef](#)] [[PubMed](#)]
159. Li, J.; Jin, H.; Zhou, H.; Rothfuss, J.; Tu, Z. Synthesis and *in vitro* biological evaluation of pyrazole group-containing analogues for PDE10A. *Med. Chem. Comm.* **2013**, *4*, 443–449. [[CrossRef](#)] [[PubMed](#)]
160. Liu, H.; Jin, H.; Yue, X.; Zhang, X.; Yang, H.; Li, J.; Flores, H.; Su, Y.; Perlmutter, J.S.; Tu, Z. Preclinical evaluation of a promising C-11 labeled PET tracer for imaging phosphodiesterase 10A in the brain of living subject. *Neuroimage* **2015**, *121*, 253–262. [[CrossRef](#)] [[PubMed](#)]

161. Hamaguchi, W.; Masuda, N.; Miyamoto, S.; Shiina, Y.; Kikuchi, S.; Mihara, T.; Moriguchi, H.; Fushiki, H.; Murakami, Y.; Amano, Y.; *et al.* Synthesis, SAR study, and biological evaluation of novel quinoline derivatives as phosphodiesterase 10A inhibitors with reduced CYP3A4 inhibition. *Bioorg. Med. Chem.* **2015**, *23*, 297–313. [[CrossRef](#)] [[PubMed](#)]
162. Hamaguchi, W.; Masuda, N.; Samizu, K.; Mihara, T.; Takama, K.; Watanabe, T. Synthesis and *in vivo* evaluation of novel quinoline derivatives as phosphodiesterase 10A inhibitors. *Chem. Pharm. Bull.* **2014**, *62*, 1200–1213. [[CrossRef](#)] [[PubMed](#)]
163. Funke, U.; Schwan, G.; Scheunemann, M.; Maisonial, A.; Hiller, A.; Fischer, S.; Deuther-Conrad, W.; Egerland, U.; Briel, D.; Nieber, K.; *et al.* Radiosynthesis, *in vitro* and *in vivo* evaluation of a 7-(2-[¹⁸F]fluoroethoxy)-6-methoxyquinazoline derivative for imaging PDE10A with PET. In Proceedings of the 19th International Symposium on Radiopharmaceutical Sciences, Amsterdam, The Netherlands, 28 August–2 September 2011; P-179, p. S268.
164. Funke, U.; Deuther-Conrad, W.; Schwan, G.; Maisonial, A.; Scheunemann, M.; Fischer, S.; Hiller, A.; Briel, D.; Brust, P. Radiosynthesis and radiotracer properties of a 7-(2-[¹⁸F]fluoroethoxy)-6-methoxy-pyrrolidinylquinazoline for imaging of phosphodiesterase 10A with PET. *Pharmaceuticals* **2012**, *5*, 169–188. [[CrossRef](#)] [[PubMed](#)]
165. Chappie, T.A.; Humphrey, J.M.; Allen, M.P.; Estep, K.G.; Fox, C.B.; Lebel, L.A.; Liras, S.; Marr, E.S.; Menniti, F.S.; Pandit, J.; *et al.* Discovery of a series of 6,7-dimethoxy-4-pyrrolidylquinazoline PDE10A Inhibitors. *J. Med. Chem.* **2007**, *50*, 182–185. [[CrossRef](#)] [[PubMed](#)]
166. Schwan, G.; Barbar Asskar, G.; Höfgen, N.; Kubicova, L.; Funke, U.; Egerland, U.; Zahn, M.; Nieber, K.; Scheunemann, M.; Sträter, N.; *et al.* Fluorine-containing 6,7-dialkoxybiaryl-based inhibitors for phosphodiesterase 10A: Synthesis and *in vitro* evaluation of inhibitory potency, selectivity, and metabolism. *Chem. Med. Chem.* **2014**, *9*, 1476–1487. [[CrossRef](#)] [[PubMed](#)]
167. Reinhardt, R.R.; Bondy, C.A. Differential cellular pattern of gene expression for two distinct cGMP-inhibited cyclic nucleotide phosphodiesterases in developing and mature rat brain. *Neuroscience* **1996**, *72*, 567–578. [[CrossRef](#)]
168. Nieber, K.; Erdmann, S.; Briel, D.; Schwan, G.; Kubicova, L.; Barbar Asskar, G.; Sträter, N.; Zahn, M.; Brust, P.; Funke, U. Neue Halogenalkoxychinazoline, deren Herstellung und Verwendung. 00401P0051DE, 20 October 2010.
169. Malamas, M.S.; Ni, Y.; Erdei, J.; Stange, H.; Schindler, R.; Lankau, H.-J.; Grunwald, C.; Fan, K.Y.; Parris, K.; Langen, B.; *et al.* Highly potent, selective, and orally active phosphodiesterase 10A inhibitors. *J. Med. Chem.* **2011**, *54*, 7621–7638. [[CrossRef](#)] [[PubMed](#)]
170. Wagner, S.; Scheunemann, M.; Fischer, S.; Egerland, U.; Ludwig, F.-A.; Höfgen, N.; Steinbach, J.; Brust, P. 1-Arylimidazo[1,5-a]quinoxalines as lead compounds for a PDE10A PET tracer. In Proceedings of Annual Congress of the European Association of Nuclear Medicine, Gothenburg, Sweden, 18–22 October 2014; OP163, p. S197.
171. Wagner, S.; Scheunemann, M.; Dipper, K.; Egerland, U.; Hoefgen, N.; Steinbach, J.; Brust, P. Development of highly potent phosphodiesterase 10A (PDE10A) inhibitors: Synthesis and *in vitro* evaluation of 1,8-dipyridinyl- and 1-pyridinyl-substituted imidazo[1,5-a]quinoxalines. *Eur. J. Med. Chem.* **2016**, *107*, 97–108. [[CrossRef](#)] [[PubMed](#)]
172. Wagner, S.; Kranz, M.; Hankir, M.; Deuther-Conrad, W.; Scheunemann, M.; Teodoro, R.; Wenzel, B.; Fischer, S.; Egerland, U.; Fenske, W.K.; *et al.* Evaluation of the new radioligand [¹⁸F]AQ-28A by small animal PET/MR demonstrates increase of PDE10A expression in striatum and brown adipose tissue (BAT) of obese mice. In Proceedings of the 21st International Symposium on Radiopharmaceutical Sciences, Columbia, MO, USA, 26–31 May 2015; 52, p. S52.
173. Wagner, S.; Teodoro, R.; Deuther-Conrad, W.; Kranz, M.; Scheunemann, M.; Fischer, S.; Wenzel, B.; Egerland, U.; Hoefgen, N.; Steinbach, J.; *et al.* Radiosynthesis and biological evaluation of the new PDE10A radioligand [¹⁸F]AQ28A. *J. Label. Comp. Radiopharm.* **2015**. submitted.
174. Nawrocki, A.R.; Rodriguez, C.G.; Toolan, D.M.; Price, O.; Henry, M.; Forrest, G.; Szeto, D.; Keohane, C.A.; Pan, Y.; Smith, K.M.; *et al.* Genetic deletion and pharmacological inhibition of phosphodiesterase 10A protects mice from diet-induced obesity and insulin resistance. *Diabetes* **2014**, *63*, 300–311. [[CrossRef](#)] [[PubMed](#)]

175. Barret, O.; Thomae, D.; Alagille, D.; Lee, H.; Papin, C.; Baldwin, R.; Jennings, D.; Marek, K.; Seibyl, J.; Tamagnan, G. First *in vivo* assessment of two PDE10 tracers [¹⁸F]MNI654 and [¹⁸F]MNI659. *J. Nucl. Med.* **2012**, *53*, 361.
176. Barret, O.; Thomae, D.; Tavares, A.; Alagille, D.; Papin, C.; Waterhouse, R.; McCarthy, T.; Jennings, D.; Marek, K.; Russell, D.; *et al.* *In vivo* assessment and dosimetry of 2 novel PDE10A PET radiotracers in humans: ¹⁸F-MNI-659 and ¹⁸F-MNI-654. *J. Nucl. Med.* **2014**, *55*, 1297–1304. [[CrossRef](#)] [[PubMed](#)]
177. Russell, D.S.; Barret, O.; Jennings, D.L.; Friedman, J.H.; Tamagnan, G.D.; Thomae, D.; Alagille, D.; Morley, T.J.; Papin, C.; Papapetropoulos, S.; *et al.* The phosphodiesterase 10 positron emission tomography tracer, [¹⁸F]MNI-659, as a novel biomarker for early huntington disease. *J. Am. Med. Assoc. Neurol.* **2014**, *71*, 1520–1528. [[CrossRef](#)] [[PubMed](#)]
178. Russell, D.S.; Jennings, D.L.; Barret, O.; Tamagnan, G.D.; Carroll, V.M.; Caille, F.; Alagille, D.; Morley, T.J.; Papin, C.; Seibyl, J.P.; *et al.* Change in PDE10 across early Huntington disease assessed by [¹⁸F]MNI-659 and PET imaging. *Neurology* **2016**, *86*, 748–754. [[CrossRef](#)] [[PubMed](#)]
179. Niccolini, F.; Haider, S.; Marques, T.R.; Muhlert, N.; Tziortzi, A.C.; Searle, G.E.; Natesan, S.; Piccini, P.; Kapur, S.; Rabiner, E.A.; *et al.* Altered PDE10A expression detectable early before symptomatic onset in Huntington's disease. *Brain* **2015**, *138*, 3016–3029. [[CrossRef](#)] [[PubMed](#)]
180. Niccolini, F.; Foltynie, T.; Marques, T.R.; Muhlert, N.; Tziortzi, A.C.; Searle, G.E.; Natesan, S.; Kapur, S.; Rabiner, E.A.; Gunn, R.N.; *et al.* Loss of phosphodiesterase 10A expression is associated with progression and severity in Parkinson's disease. *Brain* **2015**, *138*, 3003–3015. [[CrossRef](#)] [[PubMed](#)]
181. Marques, T.R.; Natesan, S.; Niccolini, F.; Politis, M.; Gunn, R.N.; Searle, G.E.; Howes, O.; Rabiner, E.A.; Kapur, S. Phosphodiesterase 10A in schizophrenia: A PET study using [¹¹C]IMA107. *Am. J. Psychiat.* **2016**. [[CrossRef](#)] [[PubMed](#)]
182. Kehler, J.; Kilburn, J.P.; Estrada, S.; Christensen, S.R.; Wall, A.; Thibblin, A.; Lubberink, M.; Bundgaard, C.; Brennum, L.T.; Steiniger-Brach, B.; *et al.* Discovery and development of ¹¹C-Lu AE92686 as a radioligand for PET imaging of phosphodiesterase 10A in the brain. *J. Nucl. Med.* **2014**, *55*, 1513–1518. [[CrossRef](#)] [[PubMed](#)]
183. Bang-Andersen, B.; Kehler, J. Radiolabelled Phenylimidazole-Based Ligands. WO 2012/062319 A1, 18 May 2012.
184. Ritzén, A.; Kehler, J.; Langgård, M.; Nielsen, J.; Kilburn, J.P.; Farah, M.M. Novel Phenylimidazole Derivatives as PDE10A Enzyme Inhibitors. WO 2009/152825 A1, 23 December 2009.
185. Hwang, D.-R.; Hu, E.; Rumpf, S.; Easwaramoorthy, B.; Castrillon, J.; Davis, C.; Allen, J.R.; Chen, H.; Treanor, J.; Abi-Dargham, A.; *et al.* Initial characterization of a PDE10A selective positron emission tomography tracer [¹¹C]AMG 7980 in non-human primates. *Nucl. Med. Biol.* **2014**, *41*, 343–349. [[CrossRef](#)] [[PubMed](#)]
186. Hwang, D.-R.; Hu, E.; Allen, J.R.; Davis, C.; Treanor, J.; Miller, S.; Chen, H.; Shi, B.; Narayanan, T.K.; Barret, O.; *et al.* Radiosynthesis and initial characterization of a PDE10A specific PET tracer [¹⁸F]AMG 580 in non-human primates. *Nucl. Med. Biol.* **2015**, *42*, 654–663. [[CrossRef](#)] [[PubMed](#)]
187. Chen, H.; Lester-Zeiner, D.; Shi, J.; Miller, S.; Glaus, C.; Hu, E.; Chen, N.; Able, J.; Biorn, C.; Wong, J.; *et al.* AMG 580: A novel small molecule phosphodiesterase 10A (PDE10A) positron emission tomography tracer. *J. Pharmacol. Exp. Ther.* **2015**, *352*, 327–337. [[CrossRef](#)] [[PubMed](#)]
188. Hu, E.; Ma, J.; Biorn, C.; Lester-Zeiner, D.; Cho, R.; Rumpf, S.; Kunz, R.K.; Nixey, T.; Michelsen, K.; Miller, S.; *et al.* Rapid identification of a novel small molecule phosphodiesterase 10A (PDE10A) tracer. *J. Med. Chem.* **2012**, *55*, 4776–4787. [[CrossRef](#)] [[PubMed](#)]
189. Taniguchi, T.; Miura, S.; Hasui, T.; Halldin, C.; Stepanov, V.; Takano, A. Radiolabeled Compounds and Their Use as Radiotracers for Quantitative Imaging of Phosphodiesterase (PDE10A) in Mammals. WO 2013/027845 A1, 28 February 2013.
190. Stepanov, V.; Miura, S.; Takano, A.; Amini, N.; Nakao, R.; Hasui, T.; Nakashima, K.; Taniguchi, T.; Kimura, H.; Kuroita, T.; *et al.* Development of a series of novel carbon-11 labeled PDE10A inhibitors. *J. Label. Comp. Radiopharm.* **2015**, *58*, 202–208. [[CrossRef](#)] [[PubMed](#)]
191. Harada, A.; Suzuki, K.; Miura, S.; Hasui, T.; Kamiguchi, N.; Ishii, T.; Taniguchi, T.; Kuroita, T.; Takano, A.; Stepanov, V.; *et al.* Characterization of the binding properties of T-773 as a PET radioligand for phosphodiesterase 10A. *Nucl. Med. Biol.* **2015**, *42*, 146–154. [[CrossRef](#)] [[PubMed](#)]

192. Takano, A.; Stepanov, V.; Gulyás, B.; Nakao, R.; Amini, N.; Miura, S.; Kimura, H.; Taniguchi, T.; Halldin, C. Evaluation of a novel PDE10A PET radioligand, [^{11}C]T-773, in nonhuman primates: Brain and whole body PET and brain autoradiography. *Synapse* **2015**, *69*, 345–355. [[CrossRef](#)] [[PubMed](#)]
193. Tóth, M.; Haggkvist, J.; Stepanov, V.; Takano, A.; Nakao, R.; Amini, N.; Miura, S.; Kimura, H.; Taniguchi, T.; Gulyas, B.; *et al.* Molecular imaging of PDE10A knockout mice with a novel PET radiotracer: [^{11}C]T-773. *Mol. Imaging Biol.* **2015**, *17*, 445–449. [[CrossRef](#)] [[PubMed](#)]
194. Takano, A.; Stepanov, V.; Nakao, R.; Amini, N.; Gulyás, B.; Kimura, H.; Halldin, C. Brain PET measurement of PDE10A occupancy by TAK-063, a new PDE10A inhibitor, using [^{11}C]T-773 in nonhuman primates. *Synapse* **2016**. [[CrossRef](#)] [[PubMed](#)]
195. Kunitomo, J.; Yoshikawa, M.; Fushimi, M.; Kawada, A.; Quinn, J.F.; Oki, H.; Kokubo, H.; Kondo, M.; Nakashima, K.; Kamiguchi, N.; *et al.* Discovery of 1-[2-fluoro-4-(1H-pyrazol-1-yl)phenyl]-5-methoxy-3-(1-phenyl-1H-pyrazol-5-yl)pyridazin-4(1H)-one (TAK-063), a highly potent, selective, and orally active phosphodiesterase 10A (PDE10A) inhibitor. *J. Med. Chem.* **2014**, *57*, 9627–9643. [[CrossRef](#)] [[PubMed](#)]
196. Cox, C.D.; Hostetler, E.D.; Flores, B.A.; Evelhoch, J.L.; Fan, H.; Gantert, L.; Holahan, M.; Eng, W.; Joshi, A.; McGaughey, G.; *et al.* Discovery of [^{11}C]MK-8193 as a PET tracer to measure target engagement of phosphodiesterase 10A (PDE10A) inhibitors. *Bioorg. Med. Chem. Lett.* **2015**, *25*, 4893–4898. [[CrossRef](#)] [[PubMed](#)]
197. Hostetler, E.; Cox, C.D.; Fan, H. Radiolabeled PDE10 Inhibitors. WO 2010/138577 A1, 2 December 2010.
198. Raheem, I.T.; Breslin, M.J.; Fandozzi, C.; Fuerst, J.; Hill, N.; Huszar, S.; Kandebo, M.; Kim, S.H.; Ma, B.; McGaughey, G.; *et al.* Discovery of tetrahydropyridopyrimidine phosphodiesterase 10A inhibitors for the treatment of schizophrenia. *Bioorg. Med. Chem. Lett.* **2012**, *22*, 5903–5908. [[CrossRef](#)] [[PubMed](#)]
199. Hostetler, E.D.; Fan, H.; Joshi, A.D.; Zeng, Z.; Eng, W.; Gantert, L.; Holahan, M.; Meng, X.; Miller, P.; O'Malley, S.; *et al.* Preclinical characterization of the phosphodiesterase 10A PET tracer [^{11}C]MK-8193. *Mol. Imaging Biol.* **2015**. [[CrossRef](#)] [[PubMed](#)]
200. Lin, J.H.; Lu, A.Y.H. Role of pharmacokinetics and metabolism in drug discovery and development. *Pharmacol. Rev.* **1997**, *49*, 403–449. [[PubMed](#)]
201. Jakobsen, S.; Kodahl, G.M.; Olsen, A.K.; Cumming, P. Synthesis, radiolabeling and *in vivo* evaluation of [^{11}C]RAL-01, a potential phosphodiesterase 5 radioligand. *Nucl. Med. Biol.* **2006**, *33*, 593–597. [[CrossRef](#)] [[PubMed](#)]



© 2016 by the authors; licensee MDPI, Basel, Switzerland. This article is an open access article distributed under the terms and conditions of the Creative Commons Attribution (CC-BY) license (<http://creativecommons.org/licenses/by/4.0/>).